Thermal Science and Engineering Progress 55 (2024) 102976

Contents lists available at ScienceDirect

Thermal Science and Engineering Progress

journal homepage: www.sciencedirect.com/journal/thermal-science-and-engineering-progress

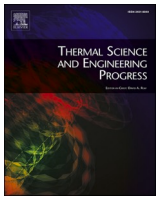

Exergoeconomic optimization of a proposed novel combined solar powered electricity and high-capacity cooling load production system for economical and potent generation via utilization of low-grade waste heat source

Asli Tiktas [a,*], Huseyin Gunerhan [b], Arif Hepbasli [c]

[a] Department of Mechanical Engineering, Faculty of Engineering-Architecture, Kırşehir Ahi Evran University, 40100 Bağbaşı, Kırşehir, Turkey
[b] Department of Mechanical Engineering, Faculty of Engineering, Ege University, 35100 Bornova, Izmir, Turkey
[c] Department of Energy Systems Engineering, Faculty of Engineering, Yasar University, 35100 Bornova, Izmir, Turkey

ARTICLE INFO

Keywords:
Absorptional cooling cycle
Organic Rankine cycle
Solar energy
Absorptional heat transformer
Life cycle cost
Exergoeconomic optimization

ABSTRACT

A novel system for combined electricity and cooling generation was introduced, integrating Flat Plate Solar Collectors (FPSC), Absorptional Heat Transformer (AHT), Organic Rankine Cycle (ORC), and Absorption Cooling Cycle (ACC) systems to utilize low-grade solar energy. The ability to use low-grade waste heat sources (70 °C–90 °C) via FPSC system for high-capacity integrated cooling and electricity generation in a more economical way, a feature not commonly addressed in conventional systems and previous literature studies, was a key advancement. The need for additional generators, boilers, and high-temperature heat sources was eliminated, resulting in substantial cost savings and a simplified system design. The FPSC-AHT integration, identified as having significant advantages over separate electricity and cooling load production, was comprehensively evaluated for its combined exergoeconomic and environmental benefits in multigeneration system design. The modeling was performed using Engineering Equation Solver (EES) and Transient System Simulation Software (TRNSYS) in Izmir, Turkey, with the aim of achieving the heightened economic efficiency and superior Coefficient of Performance (COP) values without high-temperature waste heat sources. Three configurations were examined, with the third demonstrating superior technoeconomic performance due to the increased thermal efficiency of solar hybrid photovoltaic-thermal (PV-T) systems. The higher cost per unit area in the PV-T system was effectively offset by the substantial electricity consumption, contributing to energy savings. Economic indicators for the third configuration included an initial investment of US$9.91 million, annual operational costs of US$1.29 million, a payback period of 4.2 years, an annual energy cost gain of US$9.25 million, a levelized cost of cooling (LCC) of US$0.014/kWh, and an electricity cost (LCE) of US$0.015/kWh. Through exergy analysis, toluene was identified as the optimal working fluid, revealing a total exergy destruction rate of 13245.46 kW. The performance of the proposed system was tested under different operation conditions, and based on these results, a sensitivity analysis and a comparison with the real-word studies were performed. In comparison to real-world data, the proposed system exhibits superior performance metrics, especially in terms of COP and exergy efficiency values. The optimal configuration, established using single and multiobjective optimization approaches based on exergoeconomic parameters, indicated annual electricity and cooling load production of 40000 MWh and 300 GWh, respectively. The system's efficiency in producing 1000 kW of electricity power and 4000 kW of cooling load at a comparable cost to systems generating only one output was highlighted. To determine the technoeconomic performance improvement of the proposed integrated system, the optimal configuration of the novel integrated system was compared to a reference plant for similar-scaled integrated power and cooling generation (UCI Trigeneration Plant). Compared to the UCI Trigeneration Plant, the proposed system demonstrated significant improvements in technoeconomic performance. Specifically, the proposed system achieved a 164.13 % increase in annual electricity production, a 97.38 % increase in annual cooling duty, a 60.36 % reduction in initial investment, a 57 % reduction in annual operational costs, and a 47.5 % reduction in payback period. Additionally, the levelized costs of electricity and cooling were 40 % and 22.22 % lower,

* Corresponding author.
E-mail address: asli.tiktas@ahievran.edu.tr (A. Tiktas).

https://doi.org/10.1016/j.tsep.2024.102976
Received 3 March 2024; Received in revised form 26 August 2024; Accepted 8 October 2024
Available online 15 October 2024

respectively. Significantly higher electricity and cooling output highlights the system's ability to meet demanding energy needs. Lower initial investment and operational costs, coupled with a reduced payback period, make the system financially attractive. Lower levelized costs for electricity and cooling increase the system's competitiveness and affordability. The innovative integration of technologies provides new insights into the design of multigeneration systems, setting a new benchmark for sustainable energy solutions.

Nomenclature

Symbols

b	exergy value per mole of a chemical compound, expressed in kilowatts per mole, kW/mol
CC	capital cost, US$.
E	equivalent exergy, kJ
$\dot{E}$	exergy rate, kW
h	amount of enthalpy, expressed in kilojoules per kilogram, kJ/kg, for a specific substance or system.
$\dot{m}$	mass flow rate, kg/s
N	total number of components.
$\dot{Q}$	heat transfer rate, kW
s	measure of entropy for a specific substance, typically expressed in kilojoules per kilogram per Kelvin, kJ/kg·K
T	temperature, ^{o}C or K
x	weight percentage of lithium bromide (LiBr) in a solution or substance.
z	ratio of the number of moles of a specific component to the total number of moles in a mixture or solution, often expressed as a decimal or fraction.

Subscripts

0	dead-state
c	capital
ex	exergetic
F	fuel
k	equipment

Superscripts

Ch	chemical
Ph	physical

Greek letters

η	efficiency

Abbreviations

ABS	absorber
ACC	absorptional cooling cycle
AHT	absorptional heat transformer
Con	condenser
EV	evaporator
FPSC	flat plate solar collector
Gen	Generator.
ORC	Organic Rankine Cycle
ORCC	Organic Rankine Cycle Condenser
ORCT	Organic Rankine Cycle Turbine
P	Pump.
PV	Photovoltaic.
PV-T	Photovoltaic thermal.
SHX	Solution heat exchanger.
V	Expansion valve.

1. Introduction

The 2023 BP energy forecast [1] indicates that the energy sector's recovery from the COVID-19 pandemic was influenced by Russia's incursion into Ukraine. Renewable energy investment is expected to rise from 15 % in 2021 to 24 % this year due to fluctuations in natural gas and oil markets. However, fossil fuels still dominate at 82 % of global primary energy consumption, down from 87 % in 2010, suggesting a slow transition that could take two centuries to phase out fossil fuels. Addressing global challenges like the energy crisis, greenhouse gas emissions, and environmental issues requires reducing reliance on fossil fuels through the integration of renewable energy sources and efficient waste heat recovery systems, especially in the industrial sector. Industrial operations, such as cooling and electricity generation, release nearly 50 % of energy as low-grade waste heat. Organic Rankine Cycle (ORC) systems can utilize this waste heat for power generation, offering a cost-effective and sustainable energy solution. ORC systems are versatile, easy to install, integrate well with renewable sources, and have low capital costs, making them a practical choice for generating electricity from low-grade waste heat while meeting high power needs [2].

Among renewable sources for ORC systems, solar energy is preferred for its easy integration and clean features. Literature studies show that for energy-efficient electricity production with solar-ORC systems, the solar energy system must provide a minimum temperature of 120 °C. Parabolic solar collectors (PSCs) and linear Fresnel solar collectors (LFSCs) meet this requirement and are widely used, though their high efficiency comes with significant installation, maintenance, and repair costs. Flat plate solar collectors (FPSCs) are less expensive but can only reach 90 °C, making them unsuitable for direct electricity generation. Therefore, solar ORC power plants typically use PSC and LFSC systems [3–6]. An exception is the recent work by Tiktas et al. [7], who proposed integrating FPSC and Absorptional Heat Transformer (AHT) systems for more economical solar energy and ORC-based electricity generation. Their study showed that this integrated system could bring the ORC system's waste heat source temperature closer to that of more expensive solar systems and serve as a strong exergoeconomic alternative to existing systems.

Absorption cooling cycle (ACC) systems are widely used in industrial processes to obtain the necessary cooling load in an environmentally friendly way by utilizing low-temperature and high-density waste heat [8–10]. Nonetheless, literature reviews indicate that to meet high-capacity cooling requirements with ACC systems, the waste heat source temperature should be between 120 °C and 175 °C [11]. Due to the challenge of accessing waste heat directly within this temperature range, adopting an ACC involves integrating diverse sub-systems, resulting in elevated costs and the use of intricate equipment ([12], BOWLING GREEN STATE UNIVERSITY – CENTREX CENTRAL CHILLER PLANT – HAWA [13], Chilled Water Plant Assessment Criteria Design Cleveland Airport System [14–16], Integrated solar heating and cooling unit based on a novel zeolite chiller and heat pump [17–30]). The substantial overall system costs, exemplified by instances like US$11 million for 4000 kW cooling, stem from the demand for high waste heat temperatures (120 °C–175 °C) in integrated absorption cooling [31–38].

Moreover, achieving a COP value close to one is rare in these integrated systems, which include single-stage ACCs, due to the need to satisfy the heat input requisites of the generator and the pumping power necessary to attain the cooling load. Consequently, there is a notable gap in the literature regarding efficiently addressing high cooling loads through integrated single-stage absorption systems using lower-grade waste heat sources (70 °C–90 °C) while enhancing economic feasibility and COP values. To the current knowledge of the authors of this paper, the only study addressing this literature gap is the recently published work by Tiktas et al. [39]. They addressed this gap by developing a novel integrated system design to produce high-capacity heating and cooling loads economically and environmentally using the 70 °C–90 °C heat source provided by FPSC. In this study, FPSC, AHT, and single-stage ACC systems were intelligently integrated, resulting in an ACC that could operate without any generator. The findings are particularly striking when compared to other studies in the literature. The results of the literature research on solar-assisted electricity generation and absorption technology highlight a recent common finding. With unique system designs developed through FPSC and AHT integration, a more economical and environmental alternative can be created for desired production outputs compared to conventional systems. However, this integration has only been tested separately on electrical and absorption cooling systems, with exergoeconomic parameter comparisons made with similar-scale systems in the literature. Published benchmark results show that this integration has a strong potential. This integration also has the potential to break the tendency in the literature to use the absorption effect only on cooling systems. These results reveal a significant gap in the literature on how this integration can be used in multigeneration system designs, such as cogeneration power-cooling plants, to produce economic parameters that are efficient and practical and to determine the exergoeconomic and environmental contributions to system improvement.

Despite the presence of combined solar energy-powered ORC-ACC systems in the literature, achieving high power and cooling capacities with low-grade waste heat sources remains challenging. Complex and costly designs integrating parabolic and Fresnel collectors with various robust subsystems are prominent [40–48]. Cost-effective systems like FPSCs are typically excluded due to their low-grade heat input.

The current study addresses providing a solution to the obvious gap in the literature on integrated high-capacity electricity-cooling load generation with low-grade waste heat temperature sources, using a simpler system design and in a more economical way. The novel solution presented in this study is shaped around the integration of the recently discovered and above-mentioned advantageous FPSC-AHT-ACC systems, separately for the electricity and cooling load generation subsystems. For this purpose, a novel system design that includes the integration of FPSC, AHT, and ACC subsystems has been developed, and in this way, unlike the studies in the literature, it has been shown that integrated high-capacity electricity-cooling load production can be produced economically with low-grade waste heat temperature sources and the FPSC system, which is not technically possible to use. On the other hand, other innovative features offered by this study are to determine the exergoeconomic and environmental contributions that FPSC-AHT system integration, which has been discovered recently and has advantages over separate electricity and cooling load production, will provide in multigeneration system design. According to the authors of this paper, there are no studies examining the impact of this integration on cogeneration electricity-cooling systems. In the proposed novel system, the FPSC integration allows the AHT system to operate with lower-grade waste heat (70 °C–90 °C). This system eliminates the need for a separate generator by directly using the high-temperature LiBr-water solution from the AHT absorber in the cooling system, saving costs on boilers and additional heat sources. After cooling, the solution cycles back to the AHT absorber, completing the AHT and ORC cycles and producing a net power output of 1000 kW. Technical and economic evaluations show that this system provides cost-effective, high-capacity cooling and electricity generation. Engineering Equation Solver (EES) and Transient System Simulation Software (TRNSYS) were utilized in this study to explore configurations with FPSC, evacuated solar collector, and hybrid solar photovoltaic thermal (PV-T) systems, optimizing for exergoeconomic parameters. The proposed system was evaluated across a range of operational conditions, with subsequent sensitivity analysis and comparisons to real-world studies conducted to assess the approach's effectiveness and reliability. Compared to real-world studies, the proposed design shows enhanced performance, particularly in terms of COP and exergy efficiency, indicating its potential advantages over conventional technologies. The life cycle cost uncertainty of the preferred configuration was analyzed using the Monte Carlo method, and the system was compared with solar energy-driven sustainability indices. The optimal configuration of the proposed novel system was compared with a similar-scaled integrated power and cooling reference plant in terms of a technoeconomic point of view, and in this way the primary contributions of the proposed system were presented.

2. System description and modeling

2.1. System description

The novel system, centered on integration of FPSC, AHT, and ACC systems, to deliver substantial cooling capacity and electricity generation is presented in Fig. 1. Employing the $LiBr-H_2O$ for AHT and ACC systems, the design aimed at achieving 4 MW of cooling and 1 MW of electricity. Operation of the system only required meeting heat demands in the generator (Gen) and AHT system evaporator (EV1) through FPSC integration. The FPSC's temperature range of 70 °C–90 °C facilitated high-capacity electricity and cooling from a low-grade waste heat source. Additionally, this approach led to a reduction in ACC system costs. To further cut ACC system costs, the integration of AHT and ACC systems utilized high temperature-$LiBr-H_2O$ solution from the AHT system absorber (ABS1) before completing the cycle. This solution, after reaching the condenser, was directed to the ACC system evaporator, incorporating condensed water. Electricity production involved sending the solution from the generator back to the AHT system absorber, completing the AHT and ORC cycles post-cooling cycle. This prevented the use of the generator in the ACC system, saving costs and heat source requirements. The COP value of the ACC system increased beyond 1 due to this prevention. Temperatures for Gen and EV1 were set at 80 °C due to FPSC integration while ABS1, Condenser (Con), ACC system evaporator (EV2), absorber (ABS2), ORC turbine (ORCT) inlet, and ORC condenser (ORCC) were determined at 150 °C, 40 °C, 10 °C, 25 °C, 145 °C, and 20 °C, respectively, through a parametric study. The parametric study aimed to achieve more than 17 %–19 % and 40 %–50 % of ORC system efficiency and COP value for an absorptional cooling system based on the classic PV system, creating a competitive solar-powered cooling-power system. Unlike conventional power-cooling plants with high initial and annual costs, the aim is to produce high-capacity electricity and cooling loads economically and environmentally by integrating ACC, FPSC, ORC, and AHT systems.

2.2. Process description

Within the generator (Gen), a significant portion of water in the dilute LiBr-water solution undergoes boiling and is directed to the condenser (Con) via stream 2 to enhance the solution's concentration. The water, emerging from Con as saturated liquid through stream 3, is conveyed to EV1 through stream 4 and exits as saturated vapor. Vapor from EV1, via stream 5, is directed to ABS1. The solution, now rich in absorbent after Gen, is moved to ABS1 through a solution pump and heat exchanger. The interaction of vapor and the rich solution in ABS1 yields a high-temperature dilute LiBr-water solution. The majority of vapor in this high-temperature solution are sent to Con through stream 8, further

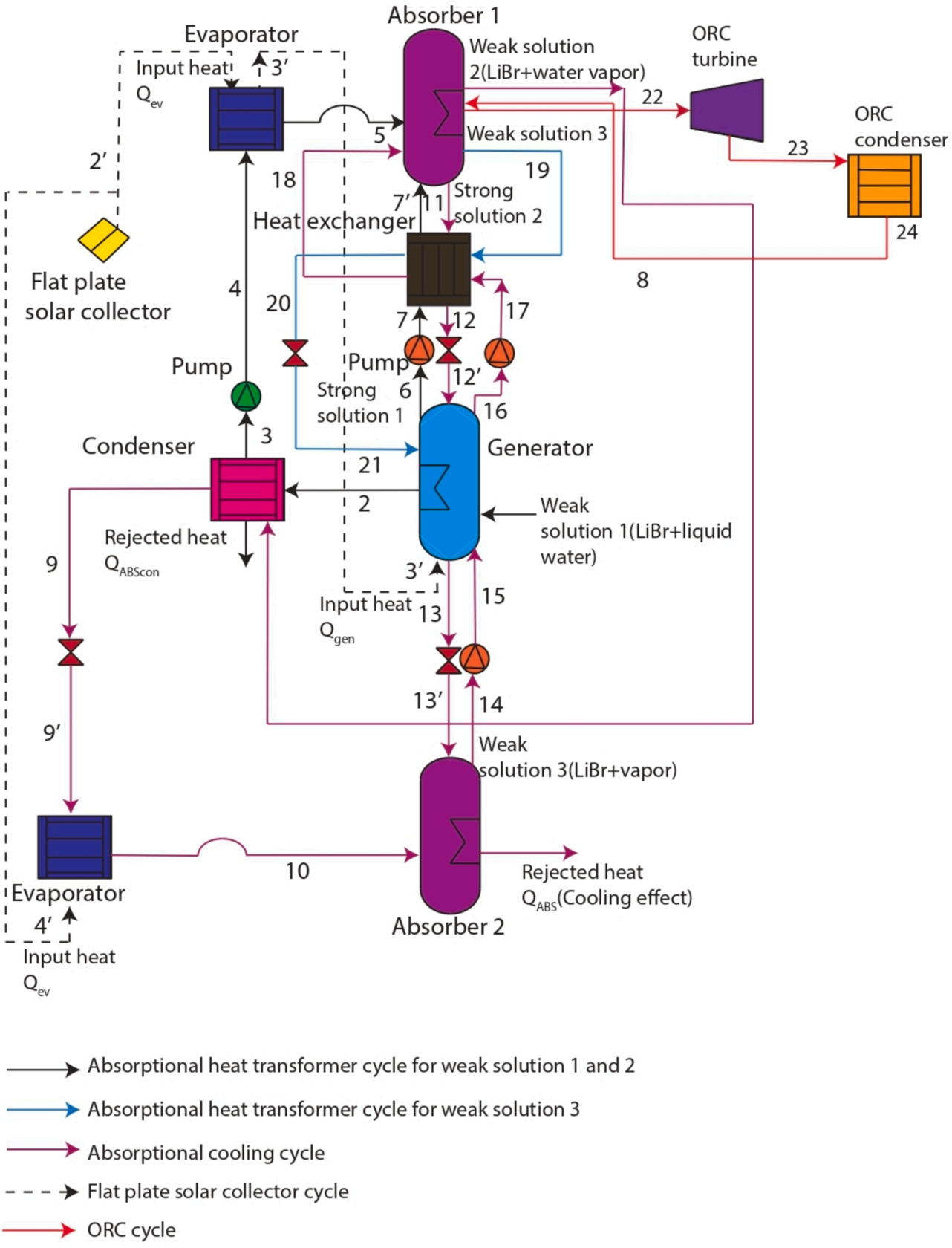

Fig. 1. Diagrammatic representation outlining the proposed system.

enriching the solution in ABS1. The pressure of the water leaving Con in the saturated liquid phase is reduced to the EV2 pressure using an expansion valve in streams 9 and 10. The saturated vapor exiting EV2 is then transferred to ABS2 through stream 11. The enriched solution from ABS1 is sent to ABS2 through streams 12 to 15. The mixing of vapor and the rich solution in ABS2 results in a dilute LiBr-water solution. This solution, conveyed to Gen through streams 16, 17, and 18, completes the absorption chiller (ACC) cycle, yielding a cooling load of 4000 kW. To achieve a net Organic Rankine Cycle Turbine (ORCT) power of 4000 kW, both the Absorption Heat Transformer (AHT) and ORC cycles must be finalized. The dilute solution sent to Gen through streams 19 and 20 is returned to ABS1 via a solution pump and heat exchanger. By transmitting the solution from ABS1 back to Gen through streams 21, the AHT cycle concludes. The ORC working fluid enters the ORC turbine at state 22 and exits at state 23, transitioning into Con. Mechanical work is generated through the expansion process in the ORC turbine. At state 24, the ORC working fluid becomes fully saturated in liquid form due to the condensation process. Subsequently, it is sent to the absorber to complete the ORC cycle, resulting in a net ORCT power of 1000 kW.

2.3. Flowsheet simulation

The thermodynamic model of the proposed novel system was formed with the integration of design parameters and special assumptions clarified in Table 1 into the EES package. Based on this model, the flowsheet simulation results are shown in Table 2. For the simulation and analysis, the established general assumptions were listed below:

a) The system operates under steady-state conditions.
b) The changes in kinetic and potential energy of the working fluids are assumed to be negligible. Because the contributions of kinetic and potential energies to the overall energy balance are typically very small compared to thermal and mechanical energies.
c) The thermal dissipation into the surroundings by the system components is disregarded.
d) Voltage variations across all components except for the pumps and valves are neglected.
e) The organic working fluid is in a saturated vapor state at the turbine inlet and in a saturated liquid state at the condenser outlet.

3. Model validation for the proposed system

The proposed system primarily incorporates an absorption heat transformer, an absorption cooling cycle, and ORC subsystems. To verify the model of the proposed system, experimental studies previously documented in the literature that focused on these cycles were selected [49–51]. The outcomes of these studies were subsequently compared with those derived from the proposed system model, with attention to net power output, energy efficiency of the ORC system, and COP for both cooling and heating applications. The design parameters for these cycles were maintained consistent with those in the chosen experimental studies during this comparison. Table 3 displays the comparison results along with the percentages of error deviation. The data clearly demonstrate that the results obtained from the proposed system model closely match with the experimental findings.

Table 2
Flowsheet simulation results.

Stream	$P[kPa]$	T [°C]	$\dot{m}[kg/s]$	$h[kJ/kg]$	$s\left[\frac{kJ}{kgK}\right]$	$X(\%)$
0	3.17	25	0.99	104.80	0.37	
1	3.17	90	0.99	2669	8.93	
2	7.38	80	0.99	2649	8.48	
3	7.38	40	0.99	167.50	0.57	
4	47.37	80	0.99	334.90	1.08	
5	47.37	80	0.99	2643	7.61	
6	47.37	140	18.08	319.30	0.73	63.49
7	39.34	135	18.08	310.10	0.70	63.49
8	7.38	140	1.62	387.40	0.31	80.25
9	7.38	40	1.62	167.50	0.57	
10	1.23	10	1.62	41.99	0.15	
11	1.23	10	1.62	2519	8.90	
12	7.38	140	19.07	387.40	0.31	80.25
13	148.30	148.30	19.07	387.40	0.63	76.08
14	150	150	19.07	337.60	0.77	63.49
15	155.40	155.40	19.07	337.60	0.99	50
16	1.23	25	20.68	45.46	0.21	46.10
17	6.07	55	20.68	113.90	0.43	46.10
18	19	80	20.68	171.30	0.60	46.10
19	137	135	20.68	299.30	0.94	46.10
20	159.30	150	20.68	311.10	0.97	46.10
21	19	80	20.68	171.30	0.60	46.10
22	2104	145	18.39	465.50	1.71	
23	75.71	20	18.39	411.20	1.72	
24	75.71	20	18.39	221	1.07	

4. Analyses

The implementation of energy analysis on this novel system involved applying mass and energy balance equations, as detailed in Table 4. The assumptions and design parameters, explicitly stated in Table 1, guided this analysis. The optimum tilt and azimuth angles in FPSC for the city of

Table 1
Design parameters and underlying assumptions for the proposed system.

Design parameters			Assumptions made		
AHT system	ACC system	ORC system	AHT system	ACC system	ORC system
Generator temperature: 80 °C	Evaporator temperature: 10 °C	ORC working fluid: Toluene	Water leaves the condenser in the saturated liquid phase.	Water leaves the condenser in the saturated liquid phase.	The organic working fluid is saturated vapor at the turbine inlet.
Condenser temperature: 40 °C	Absorber temperature: 25 °C	Evaporator temperature: 145 °C	Water leaves the evaporator in the saturated vapor phase.	Water leaves the evaporator in the saturated vapor phase.	At the Condenser outlet, the organic working fluid is in saturated liquid state.
Evaporator temperature: 80 °C	Solution heat exchanger temperature: 55 °C	Condenser temperature: 2 0 °C	LiBr-water solution separates the absorber at the absorber pressure and temperature.	LiBr-water solution separates the absorber at the absorber pressure and temperature.	
Absorber temperature: 140 °C	Refrigerant-absorbent mixture: LiBr-water solution	Turbine isentropic efficiency:0.95	LiBr-water solution separates the generator at the absorber pressure and temperature.		
Solution heat exchanger temperature: 135 °C		Output net power of turbine: 1 MW	Water separates the generator at the generator temperature.		
Refrigerant-absorbent mixture: LiBr-water solution					

Table 3
Evaluation findings from modeling the proposed system against the absorptional heat transformer, absorptional cooling and ORC systems.

Findings of the experimental studies			Findings of the proposed system			Comparison		
COP for cooling	COP for heating	Net power capacity and energy efficiency of ORC cycle, respectively	COP for cooling	COP for heating	Net power capacity and energy efficiency of ORC cycle, respectively	Error deviation of COP for cooling	Error deviation of COP for heating	Error deviation of net power capacity and energy efficiency of ORC cycle, respectively
0.335	0.45	0.3 kW and5.6 %	0.329	0.438	0.306 and 5.225 %	1.791 %	2.667 %	2.106 % and 2.385

Table 4
Mass and energy balance equations.

Equipment	Mass balance equation	Energy balance equation
Generator	$\dot{m}_{18} = \dot{m}_{13} + \dot{m}_{21}\dot{m}_{18}X_{18} = \dot{m}_{13}X_{13} + \dot{m}_{21}X_{21}$	$\dot{Q}_{gen} = \dot{m}_{18}h_{18} - \left[\dot{m}_{21}h_{21} + \dot{m}_{13}h_{13}\right]$
Condenser	$\dot{m}_2 = \dot{m}_3$	$\dot{Q}_{con} = \dot{m}_2(h_2 - h_3)$
Pump 1	$\dot{m}_3 = \dot{m}_4$	$\dot{m}_3h_3 + \dot{W}_{p1} = \dot{m}_4h_4$
Pump 2	$\dot{m}_6 = \dot{m}_7$	$\dot{m}_6h_6 + \dot{W}_{p2} = \dot{m}_7h_7$
Pump 3	$\dot{m}_{18} = \dot{m}_{19}$	$\dot{m}_{18}h_{18} + \dot{W}_{p3} = \dot{m}_{19}h_{19}$
Pump 4	$\dot{m}_{16} = \dot{m}_{17}$	$\dot{m}_{16}h_{16} + \dot{W}_{p4} = \dot{m}_{17}h_{17}$
Evaporator 1	$\dot{m}_4 = \dot{m}_5$	$\dot{Q}_{EV1} = \dot{m}_4(h_5 - h_4)$
Evaporator 2	$\dot{m}_{10} = \dot{m}_{11}$	$\dot{Q}_{EV2} = \dot{m}_{10}(h_{11} - h_{10})$
Absorber 1	$\dot{m}_{19'} = \dot{m}_{20} + \dot{m}_{12}\dot{m}_{19'}X_{19'} = \dot{m}_{20}X_{20} + \dot{m}_{12}X_{12}$	$\dot{Q}_{AB1} = \left[\dot{m}_{20}h_{20} + \dot{m}_{12}h_{12}\right] - \dot{m}_{19'}h_{19'}$
Absorber 2	$\dot{m}_{11} + \dot{m}_{15} = \dot{m}_{16}\dot{m}_{15}X_{15} = \dot{m}_{16}X_{16}$	$\dot{Q}_{AB2} = \dot{m}_{16}h_{16} - \left[\dot{m}_{11}h_{11} + \dot{m}_{15}h_{15}\right]$
Solution heat Exchanger 1	$\dot{m}_{12} = \dot{m}_{12'}\dot{m}_{20} = \dot{m}_{20'}\dot{m}_7 = \dot{m}_{7'}\dot{m}_{12}X_{12} = \dot{m}_{12'}X_{12'}\dot{m}_{20}X_{20} = \dot{m}_{20'}X_{20'}\dot{m}_7X_7 = \dot{m}_{7'}X_{7'}$	$\dot{m}_{20}h_{20} + \dot{m}_7h_7 + \dot{m}_{12'}h_{12'} = \dot{m}_{20'}h_{20'} + \dot{m}_{7'}h_{7'} + \dot{m}_{12}h_{12}$
Solution heat exchanger 2	$\dot{m}_{17} = \dot{m}_{18}\dot{m}_{13} = \dot{m}_{14}\dot{m}_{17}X_{17} = \dot{m}_{18}X_{18}\dot{m}_{13}X_{13} = \dot{m}_{14}X_{14}$	$\dot{m}_{13}h_{13} + \dot{m}_{17}h_{17} = \dot{m}_{18}h_{18} + \dot{m}_{14}h_{14}$
Expansion valve 1	$\dot{m}_{20'} = \dot{m}_{21}$	$h_{20'} = h_{21}$
Expansion valve 2	$\dot{m}_{12'} = \dot{m}_{13}$	$h_{12'} = h_{13}$
Expansion valve 3	$\dot{m}_9 = \dot{m}_{10}$	$h_9 = h_{10}$
Expansion valve 4	$\dot{m}_{14} = \dot{m}_{15}$	$h_{14} = h_{15}$
Turbine	$\dot{m}_{22} = \dot{m}_{23}$	$\dot{m}_{22}h_{22} = \dot{m}_{23}h_{23} + \dot{W}_t$
ORC condenser	$\dot{m}_{23} = \dot{m}_{24}$	$\dot{Q}_{ORC,con} = \dot{m}_{22}(h_{23} - h_{24})$
Flat plate solar collector	$\dot{m}_1 = \dot{m}_{2'}$	$\dot{Q}_y = \dot{m}_{2'}c_p(T_{2'} - T_1)$

where $\dot{m}[kg/s], X(\%), T[^\circ C], h[kJ/kg], \dot{W}_p[kW], \dot{W}_t[kW], c_p, \dot{Q}[kW]$, and f are mass flow rate, LiBr concentration in solution, temperature, specific enthalpy for streams, pump and turbine power, specific heat of working fluid, heat transfer rate and circulation rate, respectively.

Izmir, Turkey, were established based on the developed novel model by Tiktas et al. [10]. The EES modeling was seamlessly incorporated into TRNSYS by externally invoking the integration of additional system equipment. In Fig. 2, the ORC system energy efficiency is juxtaposed for five distinct ORC working fluids to identify the most favorable one from an energetic standpoint. Toluene, isopentane, and R600 exhibit superior energetic performances in comparison to the remaining options, as illustrated in this figure. The energy analysis outcomes for the optimal ORC working fluid are further listed in Table 5. Exergy analysis was conducted on the novel system to evaluate the energy quality, aligning with the principles of the second law of thermodynamics. This assessment facilitates the seamless development of improvement potential insights based on equipment considerations. Within this analysis, equations (1)–(3) from the formulae section [52] were employed to calculate both physical and chemical exergy values. Utilizing the exergy

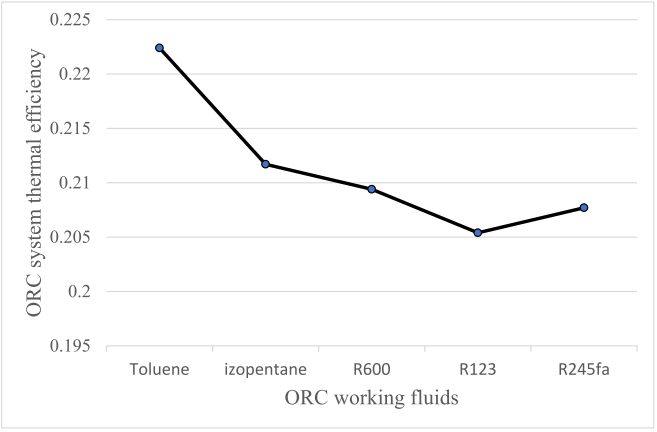

Fig. 2. Contrasting outcomes depicting the thermal efficiency of ORC system across various chosen organic Rankine cycle (ORC) working fluids.

balance equations specified in Table 6, the analysis enabled the determination of exergy destruction rates and exergy efficiency for individual components, subsystems, and the overall system.

$$\dot{E}^{Ph} = \dot{m}[(h_i - h_0) - T_0(s_i - s_0)] \quad (1)$$

$$\dot{E}^{Ch} = \sum z_i b_i \quad (2)$$

$$\dot{E} = \dot{E}^{Ph} + \dot{E}^{Ch} \quad (3)$$

Through energy and exergy analyses, an immediate evaluation of the proposed system was undertaken. However, this assessment, while insightful, fell short of providing a comprehensive understanding of the system's true performance. Consequently, a TRNSYS model was formulated, employing an illustrative example based on Izmir, to conduct annual performance simulations for the novel system. Three distinct configurations were examined and compared in the annual performance simulation. Initially, the TRNSYS model was developed to integrate FPSC, AHT, ORC, and ACC systems with external provision of electricity consumption. The annual simulation performance results of this configuration were compared with existing similar-scaled power and cooling plants separately. In the second configuration, the integration of the evacuated solar collector, AHT, ORC, and ACC systems was tested. However, in the third configuration, electricity consumption was internally met by integrating a solar hybrid PV-T system with AHT, ORC, and ACC systems. Throughout these simulations, the FPSC, evacuated solar collector, and solar hybrid PV-T components were directly sourced from the Transient System Simulation Software (TRNSYS), while other components were seamlessly integrated into TRNSYS through external calls to the Engineering Equation Solver (EES). The optimum configuration for the proposed system in terms of annual simulation performance was established. The economic evaluation and comparison of the novel system, considering three different configurations outlined in the preceding section, were conducted to illustrate the system's efficient utilization potential in comparison to similarly scaled systems. Within this assessment, factors, such as investment cost, annual operational expenses, payback period, internal rate of return, net present value, and

Table 5
Energy analysis results for the proposed novel system.

Absorptional heat transformer cycle		Absorptional cooling cycle		ORC cycle		Flat plate solar collector system	
Circulation ratio,f	18.27	Heat transfer rate in evaporator,$\dot{Q}_{EV2}[kW]$	4000	Heat transfer rate in condenser,$\dot{Q}_{ORCcon}[kW]$	3497	Required heat transfer rate in collector,$\dot{Q}_y[kW]$	9671
Heat effect coefficient,$ITK[s/kJ]$	0.465	Coefficient of performance,COP	1.01	Heat input rate in ORC cycle,$\dot{Q}_{in}[kW]$	4497	Required collector field area,$A[m^2]$	21,434
Heat transfer rate in evaporator,$\dot{Q}_{EV1}[kW]$	2284			Thermal efficiency of ORC cycle,η_{th}	0.22		
Required pump power,$\dot{W}_{P,AHT}[kW]$	2978.4						
Heat transfer rate in condenser,$\dot{Q}_{con}[kW]$		2456					
Heat transfer rate in generator,$\dot{Q}_{Gen}[kW]$		7387					

Table 6
Exergy balance equations.

Equipment	Exergy balance equation
Generator	$\dot{E}x_{d,gen} = \dot{Q}_{gen}\left(1-\frac{T_0}{T_{gen}}\right) + \left[\dot{m}_{18}\dot{E}x_{18} - \dot{m}_{21}\dot{E}x_{21} - \dot{m}_{13}\dot{E}x_{13}\right]$
Condenser	$\dot{E}x_{d,con} = -\dot{Q}_{con}\left(1-\frac{T_0}{T_{con}}\right) + \left[\dot{m}_2\dot{E}x_2 - \dot{m}_3\dot{E}x_3\right]$
Pump 1	$\dot{E}x_{d,P1} = \dot{W}_{p1} + \left[\dot{m}_3\dot{E}x_3 - \dot{m}_4\dot{E}x_4\right]$
Pump 2	$\dot{E}x_{d,P2} = \dot{W}_{p2} + \left[\dot{m}_6\dot{E}x_6 - \dot{m}_7\dot{E}x_7\right]$
Pump 3	$\dot{E}x_{d,P3} = \dot{W}_{p3} + \left[\dot{m}_{18}\dot{E}x_{18} - \dot{m}_{19}\dot{E}x_{19}\right]$
Pump 4	$\dot{E}x_{d,P4} = \dot{W}_{p4} + \left[\dot{m}_{16}\dot{E}x_{16} - \dot{m}_{17}\dot{E}x_{17}\right]$
Evaporator 1	$\dot{E}x_{d,EV,1} = \dot{Q}_{EV,1}\left(1-\frac{T_0}{T_{EV,1}}\right) + \left[\dot{m}_4\dot{E}x_4 - \dot{m}_5\dot{E}x_5\right]$
Evaporator 2	$\dot{E}x_{d,EV,2} = \dot{Q}_{EV,2}\left(1-\frac{T_0}{T_{EV,2}}\right) + \left[\dot{m}_4\dot{E}x_{10} - \dot{m}_5\dot{E}x_{11}\right]$
Absorber 1	$\dot{E}x_{d,AB1} = -\dot{Q}_{AB1}\left(1-\frac{T_0}{T_{AB1}}\right) + \left[\dot{m}_{20}\dot{E}x_{20} + \dot{m}_{12}\dot{E}x_{12} - \dot{m}_{19'}\dot{E}x_{19'}\right]$
Absorber 2	$\dot{E}x_{d,AB2} = \dot{Q}_{AB2}\left(1-\frac{T_0}{T_{AB2}}\right) + \left[\dot{m}_{16}\dot{E}x_{16} - \dot{m}_{11}\dot{E}x_{11} - \dot{m}_{15}\dot{E}x_{15}\right]$
Solution heat exchanger 1	$\dot{E}x_{d,SHX1} = \left(\dot{m}_{20}\dot{E}x_{20} + \dot{m}_7\dot{E}x_7 - \dot{m}_{12}\dot{E}x_{12}\right)$
Solution heat exchanger 2	$\dot{E}x_{d,SHX2} = \left(\dot{m}_{17}\dot{E}x_{17} - \dot{m}_{13}\dot{E}x_{13}\right)$
Expansion valve 1	$\dot{E}x_{d,V1} = \left(\dot{m}_{20'}\dot{E}x_{20'} - \dot{m}_{21}\dot{E}x_{21}\right)$
Expansion valve 2	$\dot{E}x_{d,V2} = \left(\dot{m}_{12'}\dot{E}x_{12'} - \dot{m}_{13}\dot{E}x_{13}\right)$
Expansion valve 3	$\dot{E}x_{d,V3} = \left(\dot{m}_9\dot{E}x_9 - \dot{m}_{10}\dot{E}x_{10}\right)$
Expansion valve 4	$\dot{E}x_{d,V4} = \left(\dot{m}_{14}\dot{E}x_{14} - \dot{m}_{15}\dot{E}x_{15}\right)$
Turbine	$\dot{E}x_{d,T} = \left(\dot{m}_{23}\dot{E}x_{23} - \dot{m}_{22}\dot{E}x_{22}\right) - \dot{W}_t$
ORC condenser	$\dot{E}x_{d,ORC,con} = -\dot{Q}_{ORC,con}\left(1-\frac{T_0}{T_{ORC,con}}\right) + \left[\dot{m}_{23}\dot{E}x_{23} - \dot{m}_{24}\dot{E}x_{24}\right]$
Flat plate solarcollector	$\dot{E}x_{d,FSC} = A_k I\left(1+\frac{1}{3}\left(\frac{T_0}{T_{solar}}\right)^4 - \frac{4}{3}\frac{T_0}{T_{solar}}\right) - \left[\dot{m}_{2'}c_p(T_{2'}-T_1) - T_0 ln\left(\frac{T_{2'}}{T_1}\right)\right]$

where $T_0[K]$, $T_{solar}[K]$, $A_k[m^2]$, $I[kW/m^2]$, $\dot{E}x[kW]$, and $\dot{E}x_d[kW]$ are dead-state and solar temperatures, cross-sectional area of solar collector, solar radiation density coming to the collector surface, exergy rate of streams and exergy destruction rates for equipment, respectively.

the levelized cost of electricity (LCE) and cooling duty, were considered. According to the results of the economic evaluation and comparative analysis, the third configuration of the novel system emerges as a compelling choice, presenting a robust alternative for fulfilling high-capacity cooling and electricity requirements when benchmarked against other systems. To assess the enhancement in technoeconomic performance of the proposed integrated system, the optimal configuration was benchmarked against a reference plant with similar-scale power and cooling generation capabilities [53]. The life cycle analysis was conducted to determine the total cost of the system over its entire lifespan, considering the time value of money, for the configuration of the proposed system with more favorable techno-economic parameters. To assess the uncertainty of the life cycle cost obtained from this analysis, the Monte Carlo simulation has been performed, considering variations in selected technical and economic parameters. A parametric study examined how chosen design parameters impact the ACC system COP, ORC system energy efficiency, overall system exergy efficiency, and required solar field area for the proposed novel system's optimal configuration. The performance of the proposed system was evaluated under different operation conditions. The sensitivity analysis and comparison of the real-world studies were performed. The proposed system was compared based on performance parameters related to sustainability, as presented by Chong and colleagues in their studies published in 2022 [54]. The compared system performance parameters include energy return on investment [55], carbon and water footprints Van Fan et al. [56]. Also, a more comprehensive analysis of how the proposed system aligns with global sustainability objectives was performed. The optimization of design parameters for the proposed novel system was conducted using both single and multiple objective functions, considering various exergoeconomic performance assessment criteria. These criteria encompassed energetic, exergetic, and economic parameters, focusing on the energy efficiency of the ORC system, COP for the ACC system, exergy efficiency of the overall system, total investment cost, and payback period. Different objective functions and pairs were evaluated for both single and multiobjective optimization processes, and the results were compared. The non-dominated genetic sorting algorithm (NGSA-II) was employed for this evaluation. Additionally, in the multiobjective optimization process, the optimal parameters were selected from the Pareto frontier using the Technique for Order of Preference by Similarity to Ideal Solution (TOPSIS) method.

5. Results and discussion

In Table 5, the energy analysis outcomes of the novel system are succinctly outlined. The obtained data from this analysis clearly illustrates that the heat effect coefficient of AHT, the energy efficiency of ORC, and the COP value for the cooling system stand at 0.46, 0.22, and 3.10, respectively. These values successfully achieve the objective of elevating these parameters using lower-grade waste heat sources, surpassing those of power-based and single-stage cooling systems assisted by the conventional PV system, as detailed in the introduction section. The COP result stems from the elimination of Gen in the ACC system by integrating the high-temperature LiBr-water solution from the ABS1 into the cooling system. Conversely, the energy efficiency of the ORC system improves due to the reduction in heat input, attributed to the heightened heat transfer rate in ABS1, increased mass flow rate of the ORC working fluid, and augmented net turbine power. According to the findings in this table, an expansive 21,434 m^2 of FPSC field area is necessitated for the optimal operation of the proposed system. This paper delves into the

realm of exergy, specifically establishing definitions for fuel and product exergy within the context. The proposed system design classifies net ORCT mechanical power and cooling duty as product exergy, considering them as primary outcomes. Conversely, the pumping operations are categorized as fuel exergy, given their external requirement to operate the system. Fig. 3 provides a comparative analysis of overall exergetic efficiency values for five distinct ORC working fluids, aiming to identify the most favorable option from an exergetic perspective. The detailed results for the proposed system, using toluene as the optimal working fluid, are elucidated in Table 7 and Fig. 4 through conventional exergy analysis. Table 7 explicitly indicates an entire exergy destruction rate of 13245.46 kW for the system. Further examination reveals that the exergy efficiency of the ORC and FPSC subsystems is compromised compared to other subsystems. This is attributed to the higher exergy fuel rate of solar energy for FPSC and the ORCT's incapacity to offset the negative impacts of equipment with low exergy efficiency, consequently contributing high exergy fuel values to the system. Fig. 4 illustrates the distribution of exergy destruction across the entire system, highlighting P3, V2, and Gen as major contributors with percentages of 15.93 %, 13.73 %, and 13.50 %, respectively. Conversely, Expansion Valve 3 (V3), EV1, and Con emerge as the least impactful components, accounting for rates of 0.0005 %, 0.24 %, and 0.26 %, respectively. This discrepancy is rooted in the elevated exergy fuel rate in Pump 3 (P3), Expansion Valve 2 (V2), and Gen equipment, stemming from increased heat transfer rate in Gen, entropy differences in V2, and enthalpy changes in P3 linked to LiBr concentration variations for inlet and outlet streams of the equipment.

TRNSYS simulation outcomes for the initial configuration detailed in the analysis section are depicted in Fig. 5, illustrating annual cooling duty and electricity generation. Based on these simulations, the total annual cooling duty and electricity generation are quantified at 53264.8 MWh and 270.6 GWh, respectively. A comparative assessment against similar-scale power and cooling plants is undertaken to ascertain the proposed plant's technical potential. In power plant comparison, the Saguaro, Rende, Iresen, and Ougadougou ORC solar power plants [2] serve as a reference for net ORCT mechanical power (1000 kW). For cooling plant analysis, evaluations encompass the Schüppler et al. [26] study, along with reports from Bowling Green State University central cooling [13], Cleveland Hopkins International airport chilled water [14], and ZEOSOL integrated solar heating and cooling plants [17], each with 4000 kW of cooling duty generation. The proposed system, when compared to the reference power plant study, reveals an annual electricity production 100 times higher. This outcome stems from an expanded solar field area, increased heat transfer rate in ABS1, enhanced heat input into the ORC system, and greater net obtained ORCT mechanical power. Comparison with reference cooling plant studies indicates that the annual produced cooling duty is 1.35 times

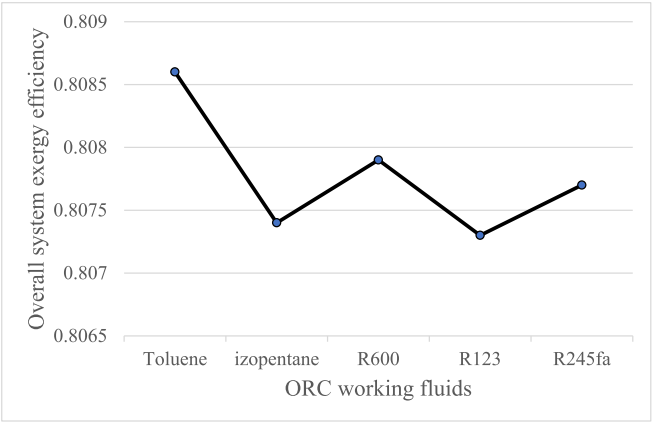

Fig. 3. Evaluating the exergy efficiency outcomes for various chosen organic Rankine cycle (ORC) working fluids within the overall proposed system.

that of the reference study, resulting from an enlarged solar field area and increased mass flow rate of the working fluid in EV2. Additionally, a reduction in the specific enthalpy of the inlet stream of Gen, attributed to decreasing LiBr concentration from the ACC system, contributes to this outcome. The third configuration's TRNSYS annual simulation results unveil an annual electricity production and consumption of 40.06 GWh and 38.48 GWh, respectively, presented in Fig. 6. This figure signifies that, with the third configuration, the proposed system's electricity consumption is entirely offset, with the surplus constituting the system's net electricity output. The costs associated with the energy and exergy flows were determined from the exergoeconomic model of the proposed system, as given in Table 8. This involved identifying the fuel and product exergy rates and their respective costs. Table 9 consolidates the economic evaluation findings based on these costs corresponding to the initial configuration of the proposed system. To assess economic aspects and facilitate the comparison with similar-scaled power and cooling plants, identical reference plants mentioned in the Annual Simulation Results in TRNSYS Modeling section were selected. Notably, existing reference power and cooling plants exhibit total initial investments and annual operation costs ranging from US$6–10 million, US $5–9 million, US$6–8 million, to US$5–7 million, respectively. Similarly, payback periods fluctuate between 10 and 15 years, and 5 and 10 years, respectively. In contrast, the proposed system's economic parameters stand at US$10.81 million for the initial total investment, US $1.41 million for annual operation costs, and a 4.27-year payback period. These results underscore the system's economic advantage, producing 1000 kW of electricity and 4000 kW of cooling load at nearly the same cost as systems generating only one of these outputs. The annual energy cost gain, levelized cost of cooling, and electricity capacities for the proposed system are determined as US$5.32 million, US $0.0204/kWh, and US$0.0283, affirming the hypothesis presented earlier. These comparisons conclusively demonstrate that integrating FPSC, AHT, ORC, and ACC with the proposed system offers a more economically viable alternative to existing cooling-electricity cogeneration systems. For the second configuration, economic evaluation results are detailed in Table 10. The economic parameters, including initial total investment and annual operation costs, payback period, annual energy cost gain, levelized cost of cooling, and electricity capacities, are reported as US$13.16 million, US$1.72 million, 5.97 years, US$2.20, US$0.052/kWh, and US$0.087/kWh, respectively. Compared to the initial configuration, with the second configuration, the high-capacity cooling and electricity outputs were produced more expensively. Because evacuated solar collectors have higher installation costs compared to the FPSC systems with higher thermal efficiency. Due to the higher thermal efficiency, the solar field area was reduced in the second configuration; however, this recovered cost from the solar field did not cover the higher installation costs. In the third configuration, the economic assessment results are summarized in Table 11. The financial indicators, which encompass the initial total investment, yearly operating costs, payback period, annual energy cost savings, and the levelized cost of cooling and electricity capacities, are reported as US$9.91 million, US$1.29 million, 4.2 years, US$9.25 million, US$0.014/kWh, and US$0.015/kWh, respectively. These findings affirm the third configuration's superior technoeconomic performance compared to reference plants and the previous configurations. This improved performance is attributed to the higher thermal efficiency of solar hybrid PV-T systems, deriving electricity and thermal energy from the same FPSC and evacuated solar collector systems fuel, leading to a reduced solar field area requirement. Despite a higher cost per unit m^2 in the PVT system, the substantial electricity consumption effectively covers this cost, with excess electricity contributing to the system as an energy-saving cost. The technoeconomic data of the optimum configuration of the proposed novel integrated system was compared with the similar-scaled integrated power-cooling generation reference plant to establish the technoeconomic contribution of the proposed system. For comparison, the UCI Trigeneration Plant in California was taken as a reference plant

Table 7
Traditional exergy analysis results of the proposed novel system.

Component	Product exergy rate,$\dot{E}x_P[kW]$	Fuel exergy rate,$\dot{E}x_F[kW]$	Exergy destruction rate,$\dot{E}x_D[kW]$	Exergetic efficiency,η_{ex}
Generator	1256	3044	1789	0.41
Condenser	123	157	33.91	0.78
Pump 1	17.34	165.70	148.4	0.10
Pump 2	40.60	165.7	125.1	0.25
Pump 3	537.2	2647	2110	0.20
Pump 4	64.52	1415	1350	0.05
Evaporator 1	356.70	388.30	31.54	0.92
Evaporator 2	141.30	209.80	68.44	0.67
Absorber 1	1307	2638	1332	0.50
Absorber 2	23.99	614.30	590.3	0.04
Solution heat exchanger 1	9560	10,098	537.2	0.95
Solution heat exchanger 2	9423	9560	137	0.99
Expansion valve 1	9560	10,161	600.10	0.94
Expansion valve 2	12,729	14,547	1818	0.88
Expansion valve 3	2.36	2.43	0.06	0.98
Expansion valve 4	9766	10,997	1231	0.88
Turbine	1000	1050	49.66	0.95
ORC condenser	44.42	58.67	14.26	0.76
Flat plate solar colector	16.01	1295	1279	0.01
Heat transformer cycle				0.822
Cooling cycle				0.818
ORC cycle				0.63
Overall system				0.81

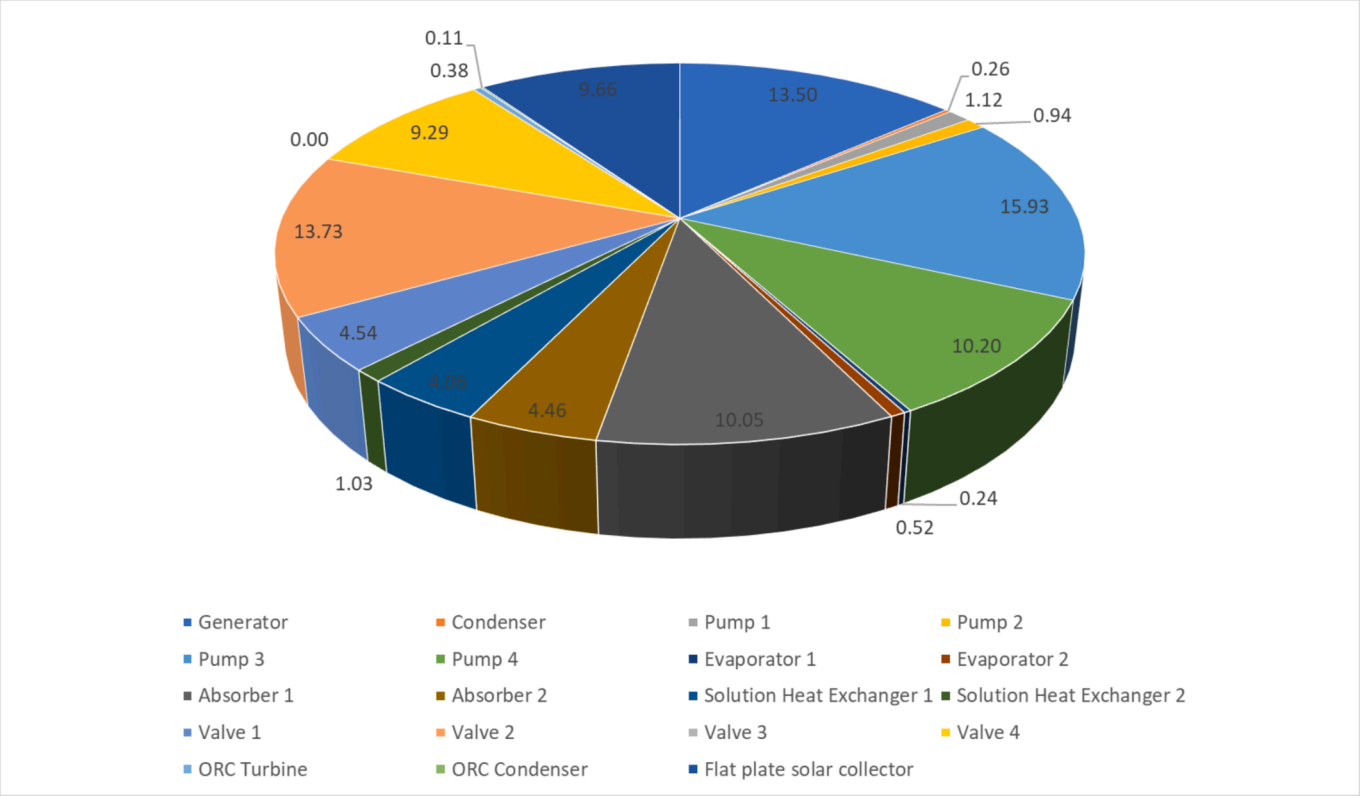

Fig. 4. Allocation of exergy dissipation rates across the entire system, categorized by the percentile contribution of each individual component.

[53]. The comparison results were presented in Table 12. According to this table, the proposed system achieved a remarkable 164.13 % increase in annual electricity production and a 97.38 % increase in annual cooling duty. This enhanced performance is indicative of the system's superior capability to meet high electricity and cooling demands efficiently. The significant boost in output suggests that the system can effectively address the energy needs of large-scale industrial and commercial applications, where traditional systems might fall short. Economically, the proposed system presented compelling advantages. The initial investment was reduced by 60.36 %, and operational costs were lowered by 57 % compared to the UCI Trigeneration Plant. These reductions translated to a faster return on investment, with the payback period being shortened by 47.5 %. Such improvements make the system an attractive option for investors and stakeholders, offering a financially viable solution for energy and cooling needs. Moreover, the levelized costs of electricity and cooling were reduced by 40 % and 22.22 %, respectively. These reductions not only enhanced the economic competitiveness of the system but also contributed to lowering the

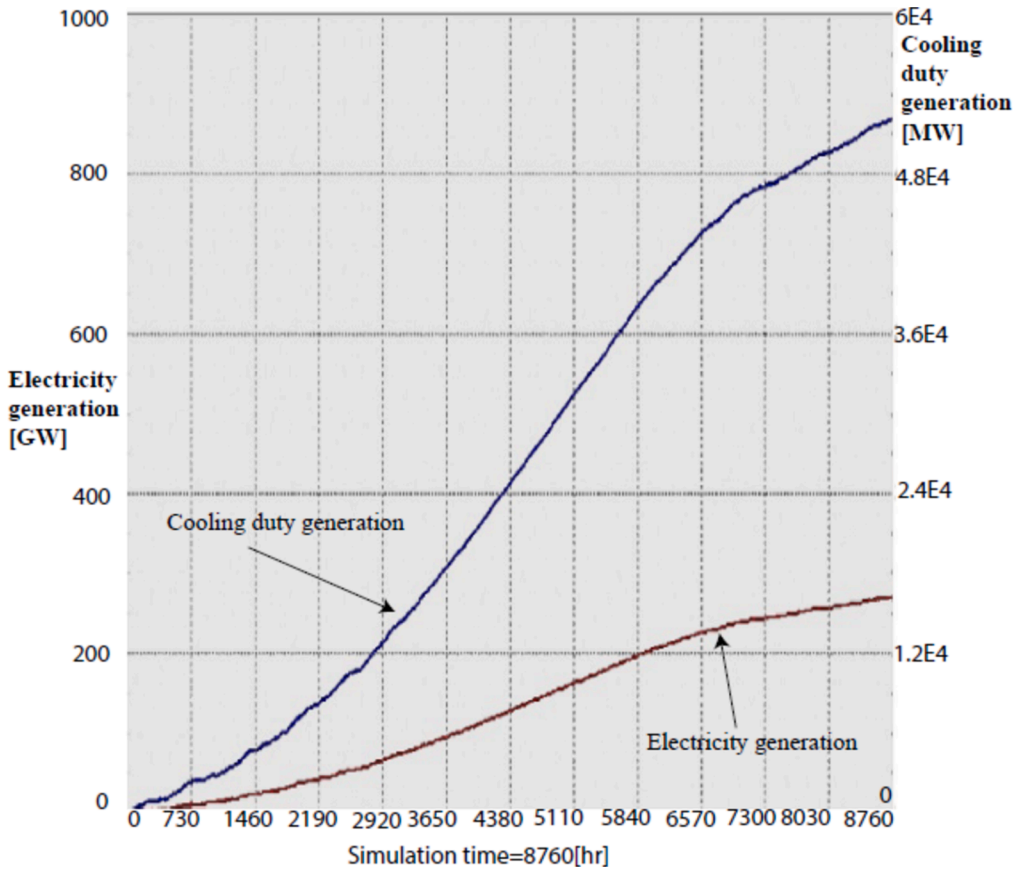

Fig. 5. Annual electricity and cooling duty generation simulation corresponding to the first configuration of the proposed system in TRNSYS for an illustrative example of Izmir, Turkey.

overall cost of energy and cooling, making it a cost-effective alternative to conventional technologies. Technologically, the proposed novel system advances the field of multigeneration systems by demonstrating the smart integration of diverse technologies. The novel combination of FPSC, AHT, ORC, and ACC establishes a new benchmark for efficient energy and cooling systems, with potential applications in various sectors including industrial facilities, commercial buildings, and remote areas with abundant solar resources. Three separate configurations of the proposed system were compared based on techno-economic parameters, and it was determined that the third configuration has more favorable parameters. For the selected configuration, the life cycle cost distribution of the recommended system is shown in Fig. 7 using the Monte Carlo method, considering changes in interest rates, PV-T system efficiency, PV-T system maintenance and repair costs, and ORCT efficiency. In the course of the parametric investigation, the effects of varying temperatures for ABS1, ABS2, Con, EV2, and ORCT on the COP of the ACC system, energy efficiency of the ORC system (η_{ORC}), overall exergy efficiency of the entire system ($\eta_{ex,overall}$), the required solar field area (RSFA), levelized costs of cooling and electricity capacities, and equivalent CO_2 emissions (EM) were explored to determine how the performance of the proposed system varied under different operating conditions. The annual dynamic performance simulation of the proposed system was performed for varying ambient temperatures and solar radiation densities in terms of exergoeconomic and environmental perspectives. These impacts and simulation results are visually represented in Figs. 8–14. As illustrated in Fig. 8, it was noted that RSFA and $\eta_{ex,overall}$ increased, while the COP value decreased and η_{ORC} remained constant with the rising temperature of ABS1. This observation is attributed to heightened pumping work in the ACC system, increased heat transfer rate in Gen, exergy product rate for the same exergy fuel rate, and a decrease in the heat transfer rate in EV1. This variation stems from the increased mass flow rate of the working fluid leaving ABS2 and the decreased mass flow rate entering EV1. Additionally, the rise in ABS1 temperature slightly raised the levelized cost of cooling due to the reduced system efficiency, necessitating more energy input per unit of cooling output. Similarly, the LCE experienced a marginal increase, as the ORC's efficiency was less affected by ABS1 temperature variations. The overall decrease in the system efficiency with higher ABS1 temperatures also led to increased CO_2 emissions per MWh of energy produced, as more fuel input was required to meet energy demands. This analysis underscores the necessity of optimizing ABS1 temperature to balance efficiency, costs, and emissions, thereby contributing to a more sustainable and economically viable system. Examining Fig. 9, it is evident that RSFA and $\eta_{ex,overall}$ increased, COP value decreased, and η_{ORC} remained constant with the escalating temperature of Con. This phenomenon is traced back to augmented pumping work in the ACC system, increased heat transfer rates in Gen and EV1, and decreased pumping work in the AHT system. The shift is influenced by the increasing mass flow rate of the working fluid leaving ABS2 and entering EV1. Furthermore, the rise in Con temperature led to noticeable changes in the system's economic and environmental performances. Specifically, levelized cost of cooling (LCC) exhibited a slight uptick due to the reduced cooling system efficiency, which required more energy input to maintain the same cooling output, thereby driving up costs. The LCE also showed a gradual increase with higher Con temperatures, although to a lesser extent, as the ORC's efficiency was only slightly impacted by Con temperature. Finally, as Con temperature increased, the CO_2 emissions per MWh of energy produced also rose, driven by the overall decline in system efficiency, which necessitated more fuel consumption to generate the same energy output. These findings highlight the importance of maintaining an optimal Con temperature to balance the system's thermal performance, economic viability, and environmental

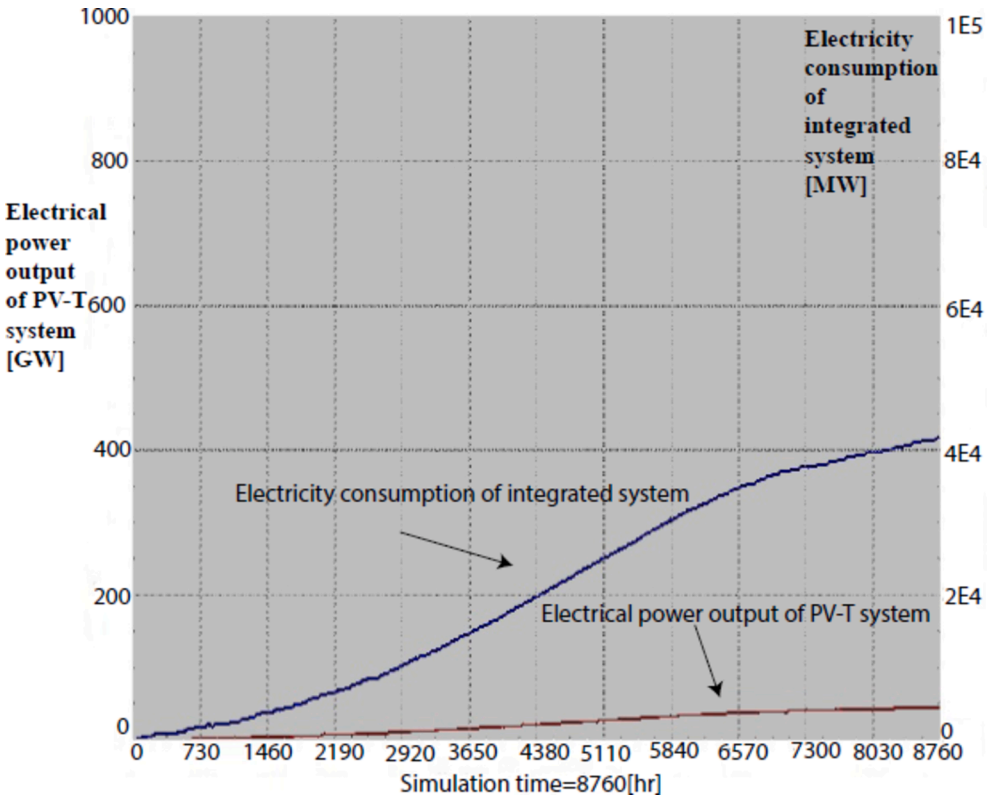

Fig. 6. Annual electricity and cooling duty generation simulation corresponding to the third configuration of the proposed system in TRNSYS for an illustrative example of Izmir, Turkey.

Table 8
Traditional exergoeconomic model equations of the proposed system.

Equipment	Exergoeconomic Cost Flow Balance Equation
Generator	$c_{18}\dot{E}x_{18} + Z_{gen} + c_{\dot{Q}_{gen}}\dot{E}_{\dot{Q}_{gen}} = c_{21}\dot{E}x_{21} + c_{13}\dot{E}x_{13}$
Condenser	$c_2\dot{E}x_2 + Z_{con} = c_{\dot{Q}_{con}}\dot{E}_{\dot{Q}_{con}} + c_3\dot{E}x_3$
Pump 1	$c_3\dot{E}x_3 + Z_{p1} + c_{\dot{W}_{P1}}\dot{W}_{p1} = c_4\dot{E}x_4$
Pump 2	$c_6\dot{E}x_6 + Z_{p2} + c_{\dot{W}_{P2}}\dot{W}_{p2} = c_7\dot{E}x_7$
Pump 3	$c_{18}\dot{E}x_{18} + Z_{p3} + c_{\dot{W}_{P3}}\dot{W}_{p3} = c_{19}\dot{E}x_{19}$
Pump 4	$c_{16}\dot{E}x_{16} + Z_{p4} + c_{\dot{W}_{P4}}\dot{W}_{p4} = c_{17}\dot{E}x_{17}$
Evaporator 1	$c_4\dot{E}x_4 + Z_{EV,1} + c_{\dot{Q}_{EV,1}}\dot{E}_{\dot{Q}_{EV,1}} = c_5\dot{E}x_5$
Evaporator 2	$c_{10}\dot{E}x_{10} + Z_{EV,2} + c_{\dot{Q}_{EV,2}}\dot{E}_{\dot{Q}_{EV,2}} = c_{11}\dot{E}x_{11}$
Absorber 1	$c_{20}\dot{E}x_{20} + c_{12}\dot{E}x_{12} + Z_{AB1} = c_{19'}\dot{E}x_{19'} + c_{\dot{Q}_{AB1}}\dot{E}_{\dot{Q}_{AB1}}$
Absorber 2	$c_{16}\dot{E}x_{16} + Z_{AB2} = c_{11}\dot{E}x_{11} + c_{15}\dot{E}x_{15} + c_{\dot{Q}_{AB2}}\dot{E}_{\dot{Q}_{AB2}}$
Solution heat exchanger 1	$c_{20}\dot{E}x_{20} + c_7\dot{E}x_7 + Z_{SHX1} = c_{12}\dot{E}x_{12}$
Solution heat exchanger 2	$c_{17}\dot{E}x_{17} + Z_{SHX2} = c_{13}\dot{E}x_{13}$
Turbine	$c_{22}\dot{E}x_{22} + Z_T = c_{23}\dot{E}x_{23} + c_{\dot{W}_T}\dot{W}_T$
ORC condenser	$c_{23}\dot{E}x_{23} + Z_{ORC,con} = c_{\dot{Q}_{ORC,con}}\dot{E}_{\dot{Q}_{ORC,con}} + c_{24}\dot{E}x_{24}$
Flat plate solar collector	$c_1\dot{E}x_1 + Z_{FSC} = c_{2'}\dot{E}x_{2'}$

where c(\$/kWh), $\dot{E}$ (kW), and $\dot{Z}$ (\$/h) are cost rate associated with exergy streams, exergy rates for streamsand heat and work interactions, and investment cost rate, respectively.

impact, ensuring sustainable and cost-effective operations. Fig. 10 reveals that RSFA increased, $\eta_{ex,overall}$ decreased, COP value decreased, and η_{ORC} remained constant with the increasing EV2 temperature. This trend is linked to intensified pumping work in the ACC system, elevated heat transfer rates in Gen and EV1, and a decrease in exergy product rate based on the declining temperature of EV2. The variation is driven by the increasing mass flow rate of the working fluid leaving ABS2 and entering EV1. Additionally, as EV2 temperature rose, its impact on the system's economic and environmental metrics became more pronounced. Specifically, LCC increased with higher EV2 temperatures due

Table 9
Economic evaluation results of the first configuration of the proposed system.

Cost of absorptional heat transformer cycle	US$3.18 million
Cost of absorptional cooling cycle	US$965.73 thousand
Cost of ORC cycle	US$499.01 thousand
Cost of electric motor	US$261.001 thousand
Electric cost	US$3.85 million
Installed cost of flat plate solar collector	US$96/$m^2$
Total direct cost	US$9.40 million
Total indirect cost	US$1.41 million
Total cost	US$10.81 million
Payback period	4.27 years
Net present value	US$5.33 million
Internal rate of return	9.39 %
Levelized cost of cooling capacity	US$0.0204 /kWh
LCE capacity	US$0.0283 /kWh
Annual operation cost	US$3.85 million
Annual energy gain cost	US$2.20 million

Table 10
Economic evaluation results of the second configuration of the proposed system.

Cost of absorptional heat transformer cycle	US$3.18 million
Cost of absorptional cooling cycle	US$965.73 thousand
Cost of ORC cycle	US$499.01 thousand
Cost of electric motor	US$261.001 thousand
Installed cost of PV	US$248/$m^2$
Total direct cost	US$11.44 million
Total indirect cost	US$1.72 million
Total cost	US$13.16 million
Payback period	5.97 years
Net present value	US$5.59 million
Internal rate of return	15.86 %
Levelized cost of cooling capacity	US$0.052 /kWh
LCE capacity	US$0.0877 /kWh
Annual energy gain cost	US$2.20 million

Table 11
Economic evaluation results of the third configuration of the proposed system.

Cost of absorptional heat transformer cycle	US$3.18 million
Cost of absorptional cooling cycle	US$965.73 thousand
Cost of ORC cycle	US$499.01 thousand
Cost of electric motor	US$261.001 thousand
Installed cost of flat plate solar collector	US$310/$m^2$
Total direct cost	US$8.62 million
Total indirect cost	US$1.29 million
Total cost	US$9.91 million
Payback period	4.20 years
Net present value	US$9.26 million
Internal rate of return	12.25 %
Levelized cost of cooling capacity	US$0.0141 /kWh
LCE capacity	US$0.0158 /kWh
Annual energy gain cost	US$2.36 million

Table 12
Technoeconomic improvement comparison results of the proposed system with the reference plant.

Metric	Proposed system finding	UCI Trigeneration Plant finding (UCI Trigeneration Plant, 2022)	Improvement of the proposed sytem
Annual Electricity Production (GWh)	396.2	150	+164.13 %
Annual Cooling Duty (MWh)	59,213.4	30,000	+97.38 %
Initial Investment (US $ million)	9.91	25	−60.36 %
Annual Operational Costs (US$ million)	1.29	3	−57 %
Payback Period (years)	4.2	8	−47.5 %
LCE (US$/kWh)	0.015	0.025	−40 %
Levelized Cost of Cooling (US $/kWh)	0.014	0.018	−22.22 %

to reduced cooling efficiency at elevated evaporator temperatures, necessitating more energy input to achieve the desired cooling output, which in turn increased costs. Similarly, the LCE saw a slight increase with rising EV2 temperatures. While (η_{ORC}), remained stable, the system's overall efficiency declined, leading to higher operational costs and a corresponding increase in LCE. The CO_2 emissions per MWh of energy produced also tended to increase with higher EV2 temperatures, as the decline in overall system efficiency required more fuel to produce the same amount of energy, resulting in higher emissions. These observations emphasize the need to optimize EV2 temperature to minimize costs and environmental impacts while maintaining system performance. In Fig. 11, it is observed that COP value and $\eta_{ex,overall}$ increased, RSFA decreased, and η_{ORC} remained constant with the rising temperature of ABS2. This shift is a result of the decreasing pumping work in the ACC system, increased heat transfer rates in Gen and EV1, and exergy fuel rate. The change is attributed to the decreasing mass flow rate of the working fluid leaving ABS2 and entering EV1. As ABS2 temperature rises, its effects on the levelized costs and CO_2 emissions also become evident. LCC decreases slightly as ABS2 temperature increases, thanks to the improved COP. As the system becomes more efficient in producing the same cooling output with less energy input, the cost per unit of cooling declines. On the other hand, LCE remains relatively stable, as the ORC efficiency does not change significantly with variations in ABS2 temperature. This stability reflects the system's ability to maintain electricity production efficiency despite changes in absorber temperature. Additionally, CO_2 emissions per MWh of energy produced tend to decrease as ABS2 temperature increases due to the enhanced cooling system efficiency, which requires less fuel input to achieve the same energy output, thereby reducing overall emissions. These findings suggest that optimizing ABS2 temperature can contribute to both economic and environmental benefits, making it a crucial parameter for sustainable system operation. Fig. 12 demonstrates that with the rising temperature of ORCT, the COP value, (η_{ORC}), and $\eta_{ex,overall}$ all increased, while RSFA decreased. This change is linked to reduced pumping work in the ACC system, elevated heat transfer rates in Gen and EV1, changes in the exergy fuel rate, andincreasedheat input into the ORC system. These variations are driven by the decreased mass flow rate of the working fluid leaving ABS2 and entering EV1, along with an increased enthalpy difference in the inlet and outlet streams of ORCT. As ORCT temperature rises, it also affects the system's economic and environmental metrics. Specifically, LCC decreases slightly with rising ORCT temperature due to the improved efficiency of the ORC system, which reduces the energy required per unit of cooling produced. This enhanced efficiency contributes to lower operational cooling costs. LCE also sees a moderate decrease as ORCT temperature increases, owing to better utilization of thermal energy in the ORC cycle, which lowers the cost per kWh of electricity generated. Lastly, CO_2 emissions per MWh of energy produced decrease with rising ORCT temperature, as the ORC system operates more efficiently at higher temperatures, reducing the fuel needed to produce the same energy output and resulting in lower emissions. These findings underscore the importance of optimizing ORCT temperature to achieve both cost-effective and environmentally sustainable operations. In Figs. 13 and 14, the annual simulation results for varying solar radiation density and ambient temperature are shown, highlighting their effects on the overall performance of the proposed system. The results of these simulations provide further insights into how environmental factors impact system efficiency and cost-effectiveness. As illustrated in Fig. 13, the higher solar radiation density leads to the increased energy production, which in turn improves

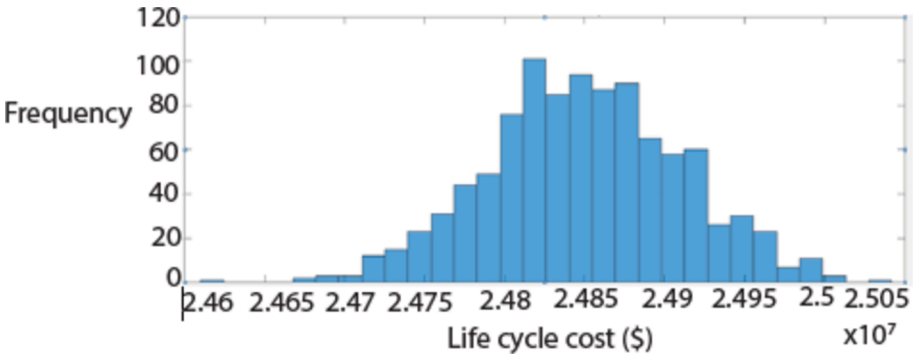

Fig. 7. Monte Carlo simulation results for the life cycle cost of the third configuration of the proposed system.

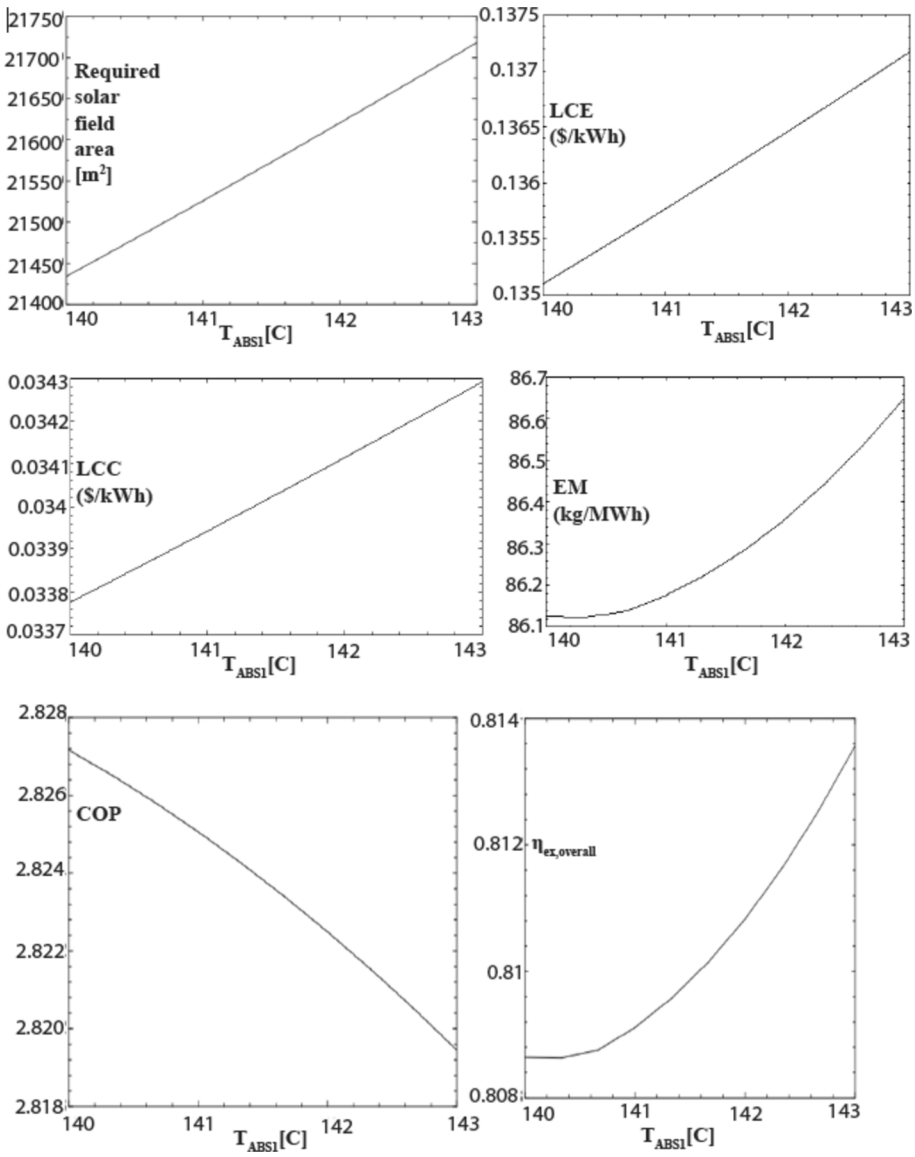

Fig. 8. Impact of ABS1 temperature on exergoenvironmental performance parameters of the proposed system.

the overall exergy efficiency and lowers LCE due to more efficient energy conversion. Specifically, when the solar radiation density increases by 10 %, energy production can increase by approximately 7 %, leading to a 5 % improvement in $\eta_{ex,overall}$ and a reduction in LCE by about 3 %. This relationship underscores the importance of maximizing solar energy capture to enhance system performance. On the other hand, Fig. 14 shows that variations in ambient temperature significantly affect the COP of the system. For instance, a 5 °C increase in ambient temperature can lead to a 10 % decrease in COP, which in turn increases LCC by around 8 % due to the higher energy input required to maintain cooling efficiency. Additionally, CO_2 emissions tend to increase with rising ambient temperatures. A 5 °C rise in ambient temperature can cause CO_2 emissions to increase by approximately 6 %, driven by the reduced system efficiency under such conditions. These annual simulation results emphasize the critical role of environmental conditions in determining the system's operational efficiency and economic viability. Optimizing both solar radiation capture and ambient temperature control can lead to significant improvements in system performance, reducing costs and emissions while enhancing energy output. To contextualize these findings, a comparison with real-world data was performed. The COP observed in the present study ranges from 2.0 to 2.8, which is higher than typical real-world systems that exhibit COP values between 0.6 and 1.6, with typical values around 1.1 to 1.4. This suggests that the proposed system might be more efficient or that the model may overestimate the system's performance compared to similar real-world systems. Real-world studies show that solar intensity significantly influences the performance of absorption cooling systems. For instance, in Jaipur, India, solar-powered absorption systems integrated with thermal energy storage were found to perform optimally during high solar intensity months, similar to our simulated data, which shows peak performance in July [57].The exergy efficiency in this study is in the range of 0.77–0.86, which is significantly higher than the exergy efficiency of real-world systems, which typically vary between 0.2 and 0.6 [58]. This discrepancy may point to differences in system design or operating conditions. ORC efficiencies in real systems are typically around 0.25 to 0.35, which is consistent with our simulation showing a peak ORC energy efficiency of 0.32 [59]. CO_2 emissions from the system varied between 84.5 and 87.5 kg/MWh, which aligns with the lower end of emissions reported for renewable energy systems in similar real-world studies, typically ranging from 50 to 150 kg/MWh Institute [60,61]. LCC for the proposed system ranges between $0.015 and $0.019/kWh, slightly lower than the global average reported by IRENA [62], which

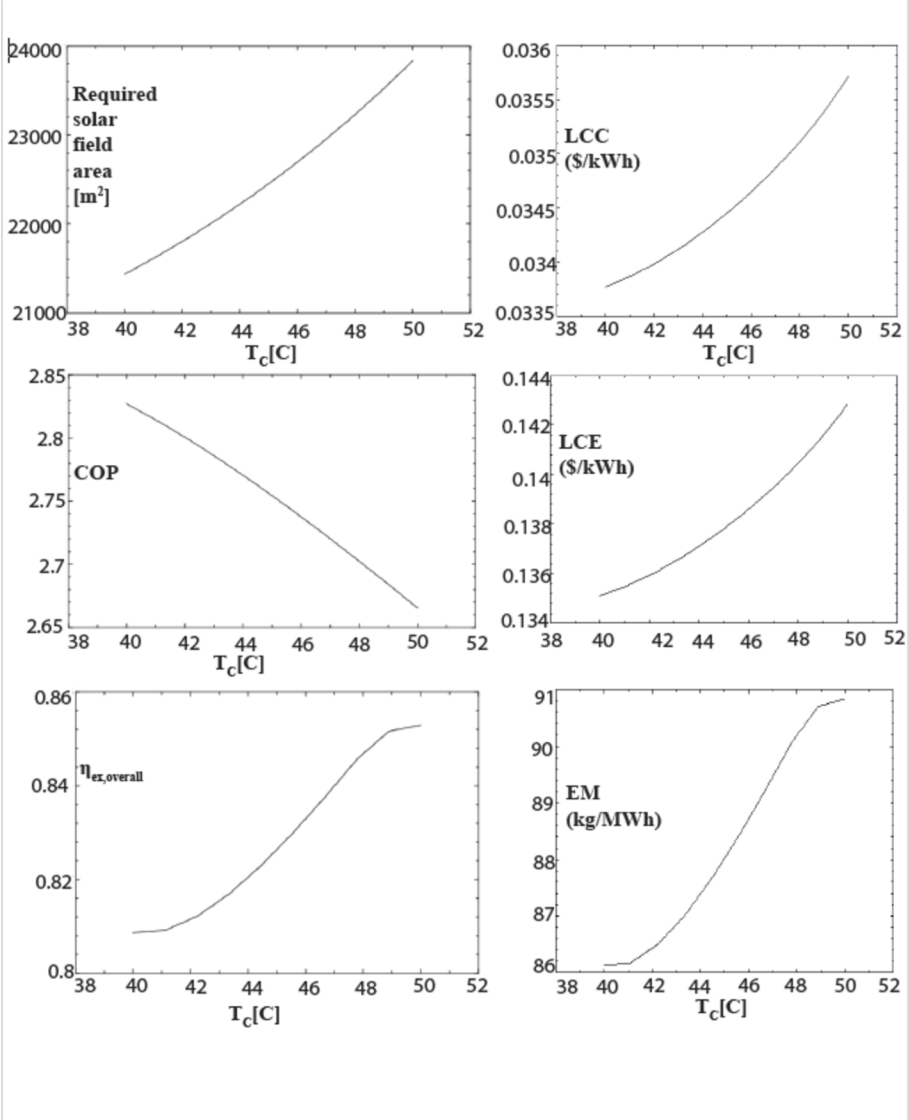

Fig. 9. Impact of Con temperature on exergoenvironmental performance parameters of the proposed system.

ranges from $0.02 to $0.08/kWh. Similarly, LCE observed in this study falls between $0.0175 and $0.0195/kWh, which is lower than the typical range reported in real-world studies, from $0.03 to $0.07/kWh Institute [60]. According to these comparison results, the proposed system showed promising performance metrics, particularly in terms of COP, exergy efficiency, and low levelized costs. In addition to the parametric analysis, a sensitivity analysis was conducted to evaluate the impact of key operational parameters, such as solar radiation density, ambient temperature, and the temperatures of ABS1, ABS2, Con, EV2, and ORCT, on the system's performance metrics. The sensitivity analysis provides valuable insights into the robustness of the proposed system under varying conditions and helps identify the most and least influential parameters. Solar radiation density was identified as one of the most influential parameters, particularly on energy production, overall exergy efficiency $\eta_{ex,overall}$, and LCE. A 10 % increase in solar radiation density resulted in a significant 7 % increase in energy production, leading to a 5 % improvement in $\eta_{ex,overall}$ and a 3 % reduction in LCE. The strong correlation between solar radiation and system performance underscores the importance of optimizing solar energy capture to enhance overall system efficiency and reduce costs. The increased availability of solar energy directly enhances the energy conversion efficiency of the ORC system, which in turn improves the overall system performance. As more energy is produced from solar input, the need for auxiliary energy sources decreases, resulting in lower operational costs and emissions. Ambient temperature also emerged as a critical factor affecting the system's COP and LCC. For instance, a 5 °C increase in ambient temperature led to a 10 % decrease in COP, which consequently increased the LCC by approximately 8 %. Additionally, CO_2 emissions increased by about 6 % due to reduced system efficiency under higher ambient temperatures. Higher ambient temperatures reduce the temperature gradient in the cooling system, requiring more energy input to maintain the same cooling output. This not only decreases the COP but also increases operational costs and emissions, highlighting the need for effective temperature control strategies. The temperature of the ORCT was found to have a moderate impact on the system's performance. Although it influenced the COP, η_{ORC}, and $\eta_{ex,overall}$, the changes were less pronounced compared to solar radiation density and ambient temperature. Specifically, a rise in ORCT temperature led to moderate improvements in COP and η_{ORC}, along with a slight decrease in RSFA. The ORC system operates more efficiently at higher ORCT temperatures, leading to better utilization of thermal energy. However, the overall impact on system performance is limited compared to other parameters, suggestingthat ORCT temperature optimization, while beneficial, is not as critical as optimizing solar input or controlling ambient temperature.

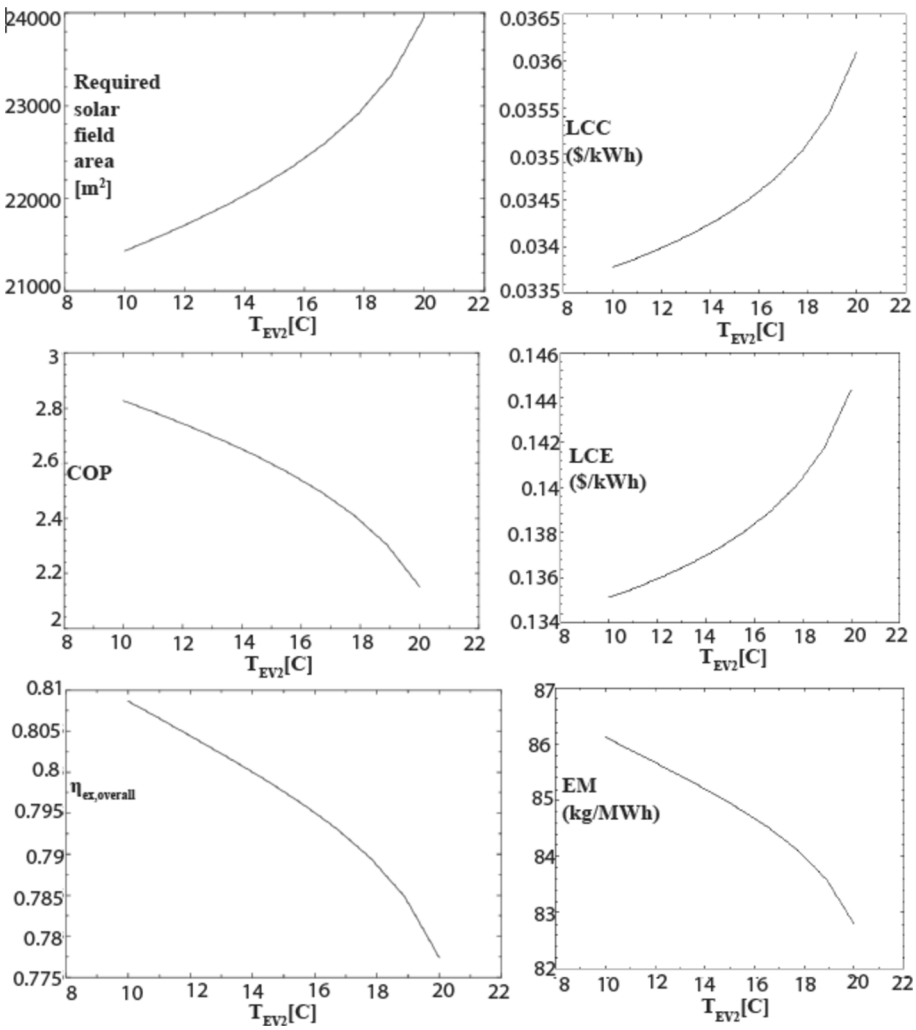

Fig. 10. Impact of EV2 temperature on exergoenvironmental performance parameters of the proposed system.

The temperature of Con had a noticeable but less significant impact on the system's LCC and LCE. While increases in Con temperature did lead to higher cooling costs and a slight rise in LCE, these effects were smaller compared to the impacts of solar radiation density and ambient temperature. Con temperature affected the ORC efficiency and the cooling system's performance, but the changes were not as dramatic. This indicates that while managing Con temperature is important, it is not the primary driver of system performance. The sensitivity analysis highlighted that solar radiation density and ambient temperature are the most critical factors influencing the performance of the proposed system. These parameters should be carefully monitored and optimized to achieve the best possible efficiency, cost-effectiveness, and environmental outcomes. In contrast, parameters like ORCT and Con temperatures, while still important, have a less pronounced effect on the overall system performance. This analysis provides a deeper understanding of how to manage the system under different operating conditions to ensure optimal performance. The selected system performance parameters related to solar energy-driven sustainability were calculated for the proposed system and compared with the reference study by Chong et al. [54] in Tables 13-14. The comparison results clearly demonstrate that the proposed system constitutes a suitable solution in terms of sustainability among solar energy-integrated systems. The system's ability to lower CO_2 emissions (84.5 to 87.5 kg/MWh) was contextualized within the broader goal of mitigating climate change, a key target of the United Nations' Sustainable Development Goal (SDG) 13, which calls for urgent action to combat climate change and its impacts. Additionally, the system's efficient use of solar energy was discussed in the context of SDG 7, which aims to ensure access to affordable, reliable, sustainable, and modern energy for all. By optimizing solar energy capture and reducing reliance on fossil fuels, the system contributes to a cleaner energy mix, promoting sustainability in energy production. The implications of the system for water sustainability were elaborated upon, particularly in terms of its reduced water consumption compared to conventional cooling systems. This aspect supports SDG 6, which focuses on ensuring the availability and sustainable management of water and sanitation for all. The proposed system's lower water usage contributes to alleviating pressure on water resources, which is especially critical in arid and semi-arid regions. Moreover, the economic viability of the system was connected to SDG 9 [63], which promotes industry, innovation, and infrastructure. The system's low levelized costs for cooling and electricity (LCC ranging from $0.015 to $0.019/kWh and LCE from $0.0175 to $0.0195/kWh) demonstrate its potential to support sustainable industrial practices and infrastructure development. The outcomes of the single-objective optimization analyses, involving various objective functions aimed at determining optimal design parameters for the proposed innovative system, are succinctly outlined in Table 15. This table encompasses the evaluation of maximizing η_{ORC}, COP, $\eta_{ex,overall}$, and minimizing both total investment cost (TIC) and payback period (PP) as respective objective functions. For maximization of η_{ORC}, the optimal design parameters were determined as (140 °C, 25 °C, 40 °C, 10 °C, 20 °C, 150 °C) for ABS1, ABS2, Con, EV2, and ORCT temperatures, respectively. This outcome is rationalized by the decrease in heat input

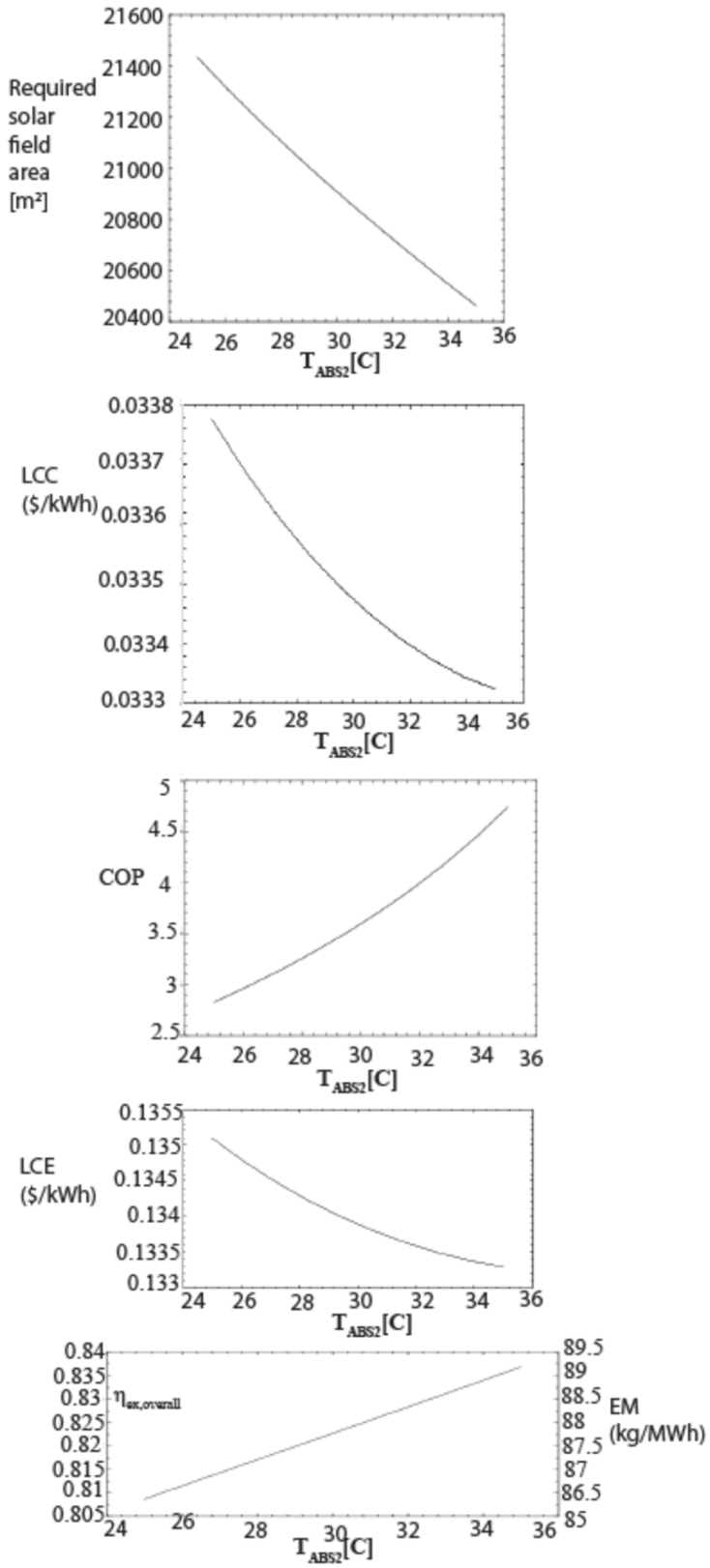

Fig. 11. Impact of ABS2 temperature on exergoenvironmental performance parameters of the proposed system.

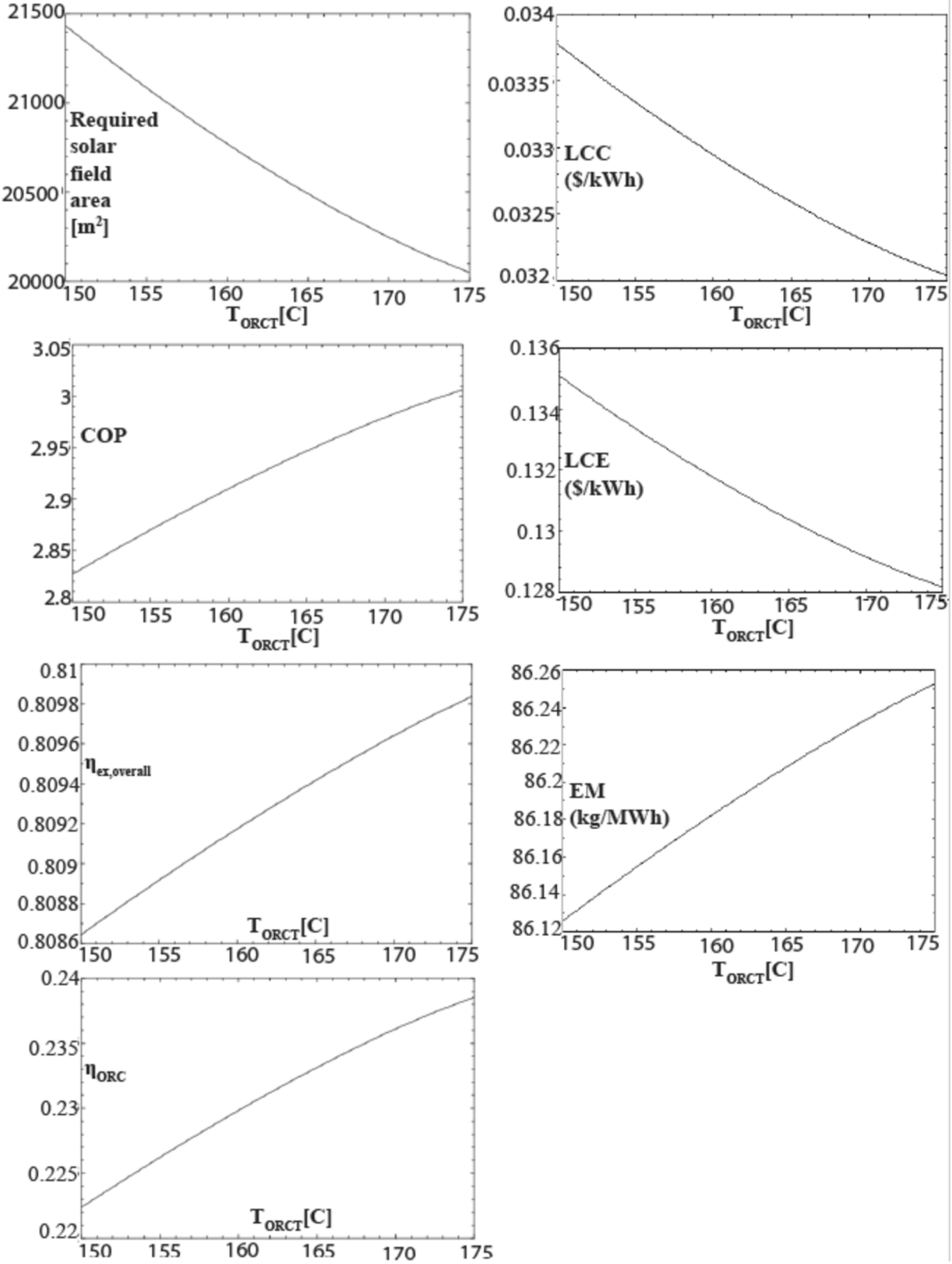

Fig. 12. Impact of ORCT temperature on exergoenvironmental performance parameters of the proposed system.

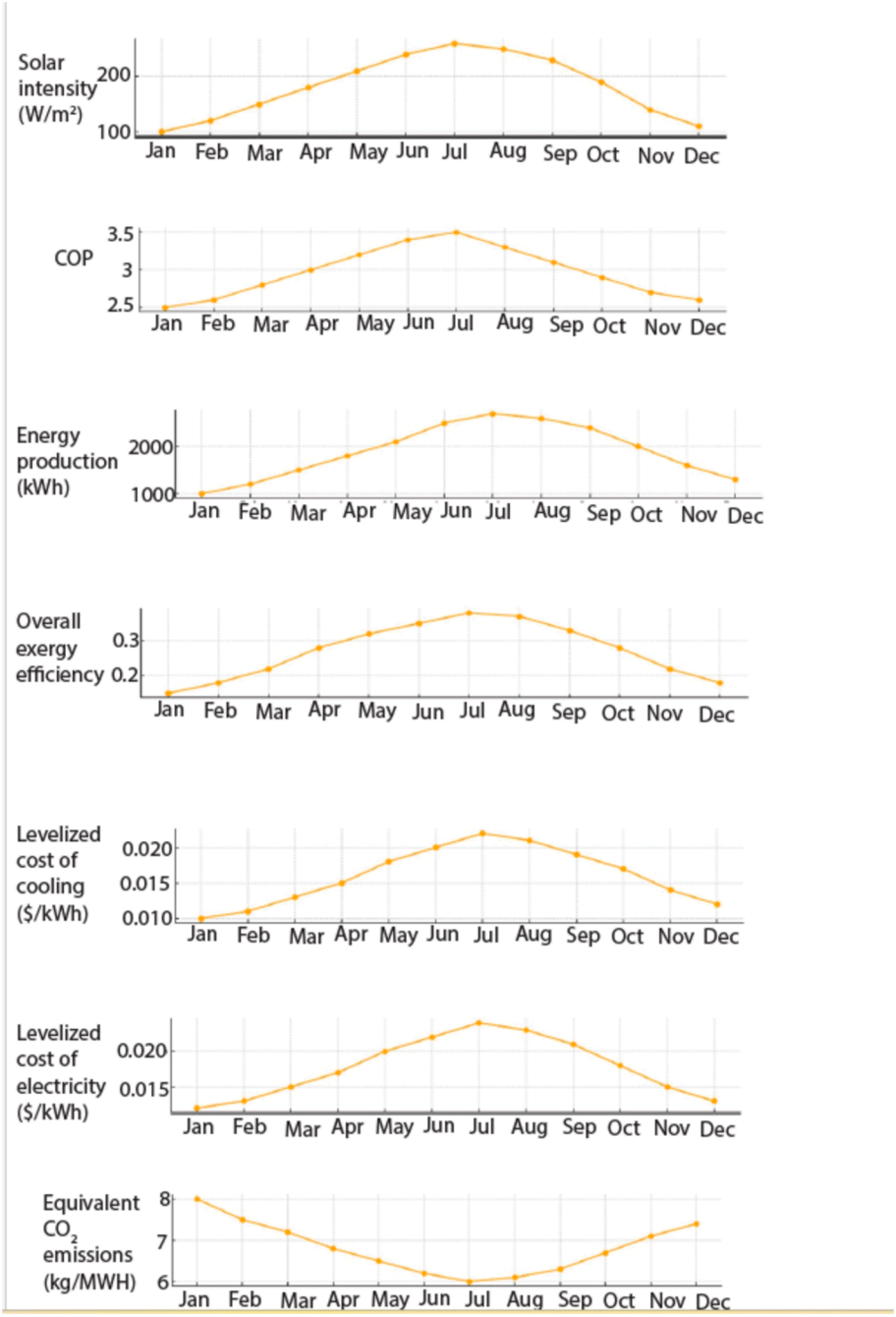

Fig. 13. Annual dynamic simulation of the proposed system for varying solar radiation densities by giving an illustrative example of city of Izmir, Turkey.

into the ORC system resulting from an increased temperature difference between ORCT and ORCC, alongside the heat input rate of the ACC system. For the maximization of COP, the optimal design parameters were identified as (138.9 °C, 33.07 °C, 50 °C, 19.07 °C, 19.8 °C, 140.5 °C). This finding can be elucidated by the reduction in pumping work in the ACC system through the decrease in enthalpy difference between the working fluid leaving ABS2 and entering Solution Heat Exchanger 2 (SHX2), as well as the mass flow rate of the working fluid leaving ABS2. To achieve the maximization of $\eta_{ex.overall}$, the optimal design parameters were established as (130.2 °C, 34.75 °C, 49.76 °C, 10.45 °C, 22.53 °C, 149.9 °C). This result is associated with the reduction in overall exergy fuel rate and an increase in overall exergy product rate. For the minimization of TIC, the optimal design parameters were set at (130 °C, 32.29 °C, 35.14 °C, 11.2 °C, 24.45 °C, 150 °C). This configuration leads to a decrease in the required solar field area and heat transfer rate in ORCC. Likewise, in minimizing PP, the optimal design parameters were determined as (130 °C, 35 °C, 35 °C, 10 °C, 15 °C, 150 °C). This outcome is associated with a decrease in TIC and an enhancement in outputs. In the multiobjective optimization process, various competing objective function pairs were selected to estimate the optimal configuration of the proposed system, as presented in Table 16. In accordance with the data presented in the table, the optimal configuration for maximizing both COP and η_{ORC} corresponds to design parameters of (140 °C, 35 °C, 48.75 °C, 24.89 °C, 15.02 °C, 150 °C). Similarly, for the joint maximization of η_{ORC} and $\eta_{ex.overall}$, the most effective design parameters were identified as (139.65 °C, 31.63 °C, 36.48 °C, 12.89 °C, 26.25 °C, 149.64 °C). To achieve the dual objective of optimizing η_{ORC} and simultaneously minimizing both PP and TIC, the optimal design parameters were determined as (130.32 °C, 25.04 °C,

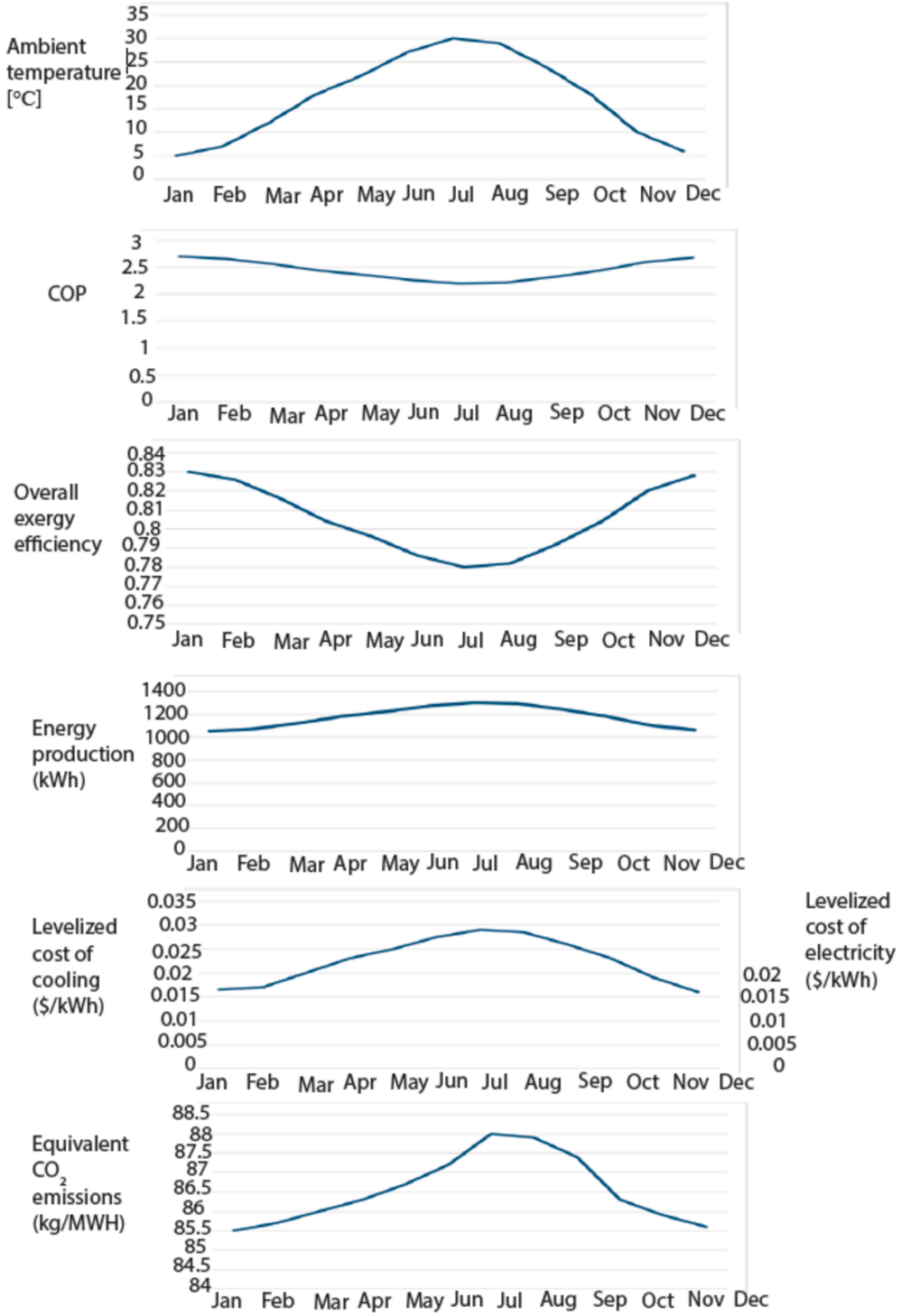

Fig. 14. Annual dynamic simulation of the proposed system for varying ambient temperature by giving an illustrative example of city of Izmir, Turkey.

Table 13
Results of the selected system performance parameters related to sustainability for the recommended system.

Energy return on investment	Carbon footprint [kg/MWh]	Water footprint [L/MWh]
4.013	86.27	111.163

Table 14
System performance parameters related to solar energy presented in the sustainability-focused reference study [54].

Energy return on investment	Carbon footprint [kg/MWh]	Water footprint [L/MWh]
1–16.1	101.5	330

Table 15
Single objective optimization results of the proposed system.

Objective function	Optimum $T_{ABS1}(^{\circ}C)$	Optimum $T_{ABS2}(^{\circ}C)$	Optimum $T_C(^{\circ}C)$	Optimum $T_{EV2}(^{\circ}C)$	Optimum $T_{ORCC}(^{\circ}C)$	Optimum $T_{ORCT}(^{\circ}C)$
Maximization of η_{ORC}	140	25	40	10	20	150
Maximization of COP	139.9	33.07	50	19.07	19.8	140.5
Maximization of $\eta_{ex,overall}$	130.2	34.75	49.76	10.45	22.53	149.9
Minimization of TIC	130	32.29	35.14	11.2	24.45	150
Minimization of PP	130	35	35	10	15	150

Table 16
Multiobjective optimization results of the proposed system.

Objective function	Optimum $T_{ABS1}(^{\circ}C)$	Optimum $T_{ABS2}(^{\circ}C)$	Optimum $T_C(^{\circ}C)$	Optimum $T_{EV2}(^{\circ}C)$	Optimum $T_{ORCC}(^{\circ}C)$	Optimum $T_{ORCT}(^{\circ}C)$
Maximization of η_{ORC} and COP	140	35	48.75	24.89	15.02	150
Maximization of η_{ORC} and $\eta_{ex,overall}$	139.65	31.63	36.48	12.89	26.25	149.64
Maximization of η_{ORC} and minimization of PP and TIC	130.32	25.04	46.04	21	30	140
Maximization of COP and of $\eta_{ex,overall}$	130	35	41.65	14.69	30	150
Maximization of COP and minimization of PP and TIC	130	34.97	40.59	10.79	15.09	149.83
Maximization of η_{ORC}, COP, $\eta_{ex,overall}$ and minimization of TIC and PP	130.18	35	42.98	24.68	15.02	150

46.04 °C, 21 °C, 30 °C, 140 °C). Furthermore, in pursuit of maximizing $\eta_{ex,overall}$ and COP, the most favorable design parameters were established as (130 °C, 35 °C, 41.65 °C, 14.69 °C, 30 °C, 150 °C). For the objective of optimizing COP while minimizing both TIC and PP, the optimal design parameters were defined as (130 °C, 34.97 °C, 40.59 °C, 10.79 °C, 15.09 °C, 149.83 °C). Lastly, to simultaneously maximize η_{ORC}, exergoeconomic factor (f), and COP, the optimal design parameters were determined as (130.18 °C, 35 °C, 42.98 °C, 24.68 °C, 15.02 °C, 150 °C). The selected parameters for annual electricity and cooling load production, totaling 396.2 GWh and 59213.4 MWh, respectively, were derived from the third configuration of the proposed system with the latte case, as indicated by TRNSYS annual simulation results. Also, the resultant optimal Pareto frontiers derived from this procedure for the latte case are depicted in Figs. 15–17.

6. Conclusions

In this study, a novel electricity-cooling cogeneration system was conceptualized and developed, integrating FPSC, AHT, ORC, and ACC systems to harness low-grade solar energy. The primary aim was to achieve high-capacity electricity and cooling duty generation while enhancing economic efficiency and achieving higher COP values without the need for high-temperature waste heat sources. Furthermore, an innovative aspect of this study is the evaluation of the combined exergoeconomic and environmental benefits provided by the FPSC-AHT system integration. This integration, recently identified as having significant advantages over the separate production of electricity and cooling loads, offers new insights into the design of multigeneration systems. The proposed system is distinct from existing medium- to high-capacity electricity-cooling plants by utilizing an innovative integration of FPSC, AHT, and single-stage ACC systems. This integration addresses a notable gap in the literature by enabling efficient and cost-effective high-capacity cooling and electricity generation using low-grade waste

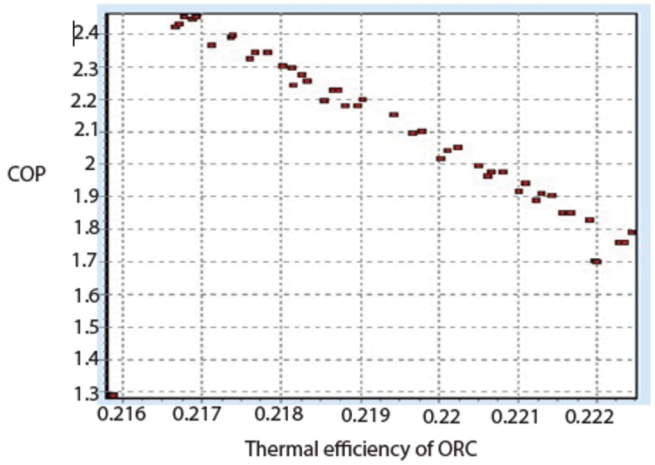

Fig. 15. Optimal Pareto frontier of COP-η_{ORC} for latte case.

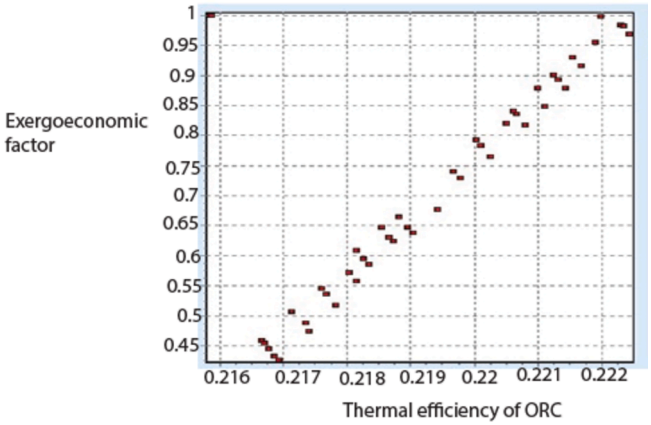

Fig. 16. Optimal Pareto frontier of f-η_{ORC} for latte case.

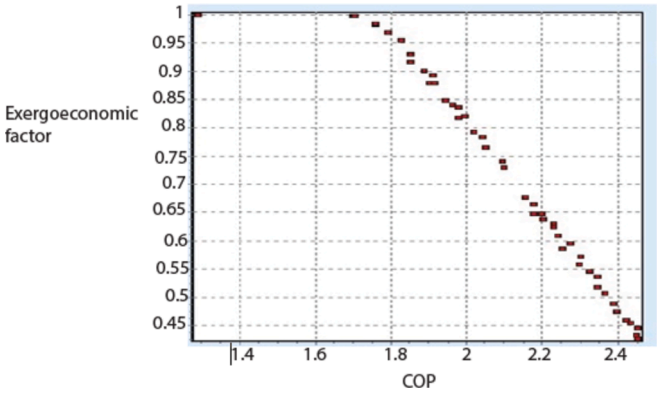

Fig. 17. Optimal Pareto frontier of f-COP for latte case.

heat sources (70 °C–90 °C), which is typically not feasible with conventional systems. The FPSC system's ability to operate with lower-grade waste heat eliminates the need for additional generators, boilers, and high-temperature heat sources, resulting in substantial cost savings. For modeling the proposed system, EES and TRNSYS were employed, focusing on a case study centered in Izmir, Turkey. The system was evaluated for three different configurations, with a targeted output of 1000 kW of mechanical ORC power and 4000 kW of cooling duty. Comparative analysis with similar-scaled cooling plants worldwide demonstrated that the proposed system offers a more economically viable alternative, with the third configuration exhibiting superior technoeconomic performance. This performance is attributed to the higher thermal efficiency of solar hybrid photovoltaic-thermal (PV-T) systems, which generate both electricity and thermal energy from the same FPSC and evacuated solar collector systems fuel, leading to a reduced solar field area requirement. Despite a higher cost per unit area in the PV-T system, the substantial electricity generation offsets this cost, contributing to overall energy savings. To establish the system's technoeconomic improvement contribution, the optimal configuration of the proposed novel integrated system was compared to the UCI Trigeneration Plant [53], a reference plant for similar-scaled integrated power and cooling generation. The results showed a remarkable 164.13 % increase in annual electricity production and a 97.38 % increase in annual cooling duty for the proposed system. Additionally, the initial investment was reduced by 60.36 %, annual operational costs by 57 %, and the payback period by 47.5 %. The levelized costs of electricity and cooling were lowered by 40 % and 22.22 %, respectively. These improvements underscore the proposed system's financial attractiveness and technological advancement, highlighting its ability to meet high electricity and cooling demands efficiently and cost-effectively. Energy and exergy analyses, along with parametric studies and exergoeconomic optimization based on single and multiobjective functions, were performed to determine the optimal design parameters of the proposed system. The proposed system's performance was assessed under various operational conditions, considering key parameters such as ABS1, ABS2, Con, EV2, ORCT temperatures, solar radiation density, and ambient temperature. The analysis yielded several critical insights into the system's exergoeconomic and environmental performance. The proposed system demonstrated a high coefficient of performance (COP), ranging from 2.0 to 2.8, which is significantly higher than the typical values observed in real-world systems (0.6 to 1.6). This suggests either an especially efficient design or a potential overestimation within the model. Furthermore, the exergy efficiency ranged from 0.77 to 0.86, surpassing typical real-world systems, where exergy efficiency typically falls between 0.2 and 0.6. These results highlight the proposed system's potential for superior performance in practical applications. The environmental impact assessment indicated that CO_2 emissions from the system ranged between 84.5 and 87.5 kg/MWh, aligning with the lower end of emissions reported for renewable energy systems, typically ranging from 50 to 150 kg/MWh. The levelized costs for cooling and electricity were found to be competitive, with LCC ranging from $0.015 to $0.019/kWh and the LCE from $0.0175 to $0.0195/kWh, which are lower than those reported in similar real-world studies. In addition to these findings, sensitivity analysis identified solar radiation density as the most influential parameter on the system's performance, particularly in terms of energy production, exergy efficiency, and LCE. A 10 % increase in solar radiation density resulted in a 7 % increase in energy production, a 5 % improvement in exergy efficiency, and a 3 % reduction in LCE. Conversely, ambient temperature had a significant impact on COP and LCC, with a 5 °C increase leading to a 10 % decrease in COP and an 8 % increase in LCC, as well as a 6 % rise in CO_2 emissions. The influence of ORCT and Con temperatures on system performance, while important, was less pronounced. An annual simulation based on these parameters affirmed the system's robustness as an alternative to existing cooling-electricity cogeneration systems in terms of both output generation and economic considerations. These findings underscore the innovative nature and practical applicability of the proposed system, providing a viable solution to the existing challenges of achieving high-capacity cooling and electricity generation using low-grade waste heat sources. This novel approach not only advances the integration of renewable energy sources with efficient waste heat recovery systems but also sets a new benchmark for future research and development in the field of sustainable energy solutions. The system's contribution to environmental concerns and sustainable development goals was taken into consideration. However, it is important to acknowledge the inherent uncertainties and complexities involved in integrating these diverse technologies. The system's performance was dependent on various operational parameters, and while the model predictions are promising, they are subject to the limitations of the simulation environment. Real-world applications may present challenges such as component degradation, fluctuating load demands, and environmental variations, which could lead to performance deviations. Additionally, the analysis relies on specific assumptions about material properties, operational efficiencies, and environmental factors that may not fully account for real-world variability. The limited availability of high-quality, site-specific data further contributes to these uncertainties. The integration of multiple technologies (FPSC, AHT, ORC, ACC) introduces complexities related to the interactions between these components. Unforeseen synergies or conflicts could arise, potentially affecting overall system performance. Moreover, the system's performance is highly sensitive to changes in operational parameters such as ambient temperature, solar radiation intensity, and component temperatures. Small variations in these parameters could lead to significant efficiency and output changes, underscoring the need for robust control strategies. Scalability and adaptability of the proposed system to different applications are all factors that introduce uncertainty. The proposed system's performance at different scales or in various geographic regions with distinct climatic conditions can differ. Managing the operation of this integrated system requires sophisticated control strategies, adding to the complexity of development, implementation, and maintenance, especially in dynamic environments with changing loads and environmental conditions. The complexity of maintenance and reliability increases with the integration of different technologies, each with unique maintenance requirements and potential failure modes. This could complicate the overall maintenance strategy and increase the likelihood of downtime or higher operational costs. Furthermore, while the levelized costs for cooling and electricity appear competitive in the modeled scenario, the real-world economic viability will depend on factors such as market conditions, energy prices, and regulatory environments, introducing economic uncertainties that could affect the feasibility of broader deployment. The main conclusion remarks are listed as follows:

a) The energy analysis results demonstrate significant enhancements in key parameters: AHT's heat effect coefficient is 0.46, the ORC system achieves an energy efficiency of 0.22, the cooling system attains a COP value of 3.10, and the required FPSC field area measures 21,434 m^2. These improvements, surpassing those of conventional systems, stem from innovative approaches, such as eliminating the ACC system's generator and integrating high-temperature LiBr-water solution from ABS1 into the cooling system, leading to increased heat transfer rates, higher ORC working fluid mass flow, and greater net turbine power.
b) Exergy analysis identifies toluene as the optimal working fluid, revealing an entire exergy destruction rate of 13245.46 kW in the proposed system. Notably, the exergy efficiencies of the ORC and FPSC subsystems are compromised due to higher exergy fuel rates from solar energy in FPSC and the ORCT's inability to offset impacts from low exergy efficiency equipment. P3, V2, and Gen as major contributors (15.93 %, 13.73 %, and 13.50 %, respectively), while V3, EV1, and Con have minimal impact (0.0005 %, 0.24 %, and 0.26

%, respectively). This discrepancy originates from elevated exergy fuel rates in P3, V2, and Gen equipment, linked to increased heat transfer rates, entropy differences, and enthalpy changes in the respective components.

c) TRNSYS simulation results for the initial proposed system configuration indicate an annual cooling duty of 53264.8 MWh and electricity generation of 270.6 GWh. Compared to a reference power plant study, the proposed system achieves a remarkable 100-fold increase in annual electricity production, driven by a larger solar field, increased heat transfer rates in ABS1, enhanced ORC system heat input, and greater net mechanical power from the ORCT. In contrast, reference cooling plant studies show a 1.35-times increase in annual cooling duty, attributed to an expanded solar field and increased working fluid mass flow in EV2, along with a decrease in Gen's inlet stream enthalpy due to reduced LiBr concentration in the ACC cycle. For the third configuration, TRNSYS annual simulation results reveal an electricity production of 40.06 GWh and consumption of 38.48 GWh, indicating that the system's electricity consumption is fully offset, with the surplus constituting the net electricity output.

d) Existing power and cooling plants typically involve initial and annual operational costs ranging from US$6–10 million, US$5–9 million, US$6–8 million, to US$5–7 million, with payback periods of 10–15 years and 5–10 years, respectively. In contrast, the proposed system demonstrates economic strength with an initial investment of US$10.81 million, annual operation costs of US$1.41 million, and a 4.27-year payback period. This underscores its efficiency in generating 1000 kW of electricity and 4000 kW of cooling load at a comparable cost to systems producing only one output. Economic metrics, including annual energy cost gain, levelized cost of cooling, and electricity capacities, are determined as US$5.32 million, US $0.0204/kWh, and US$0.0283, affirming the system's viability. The optimal configuration's economic parameters, US$9.91 million initial investment, US$1.29 million annual operation costs, 4.2-year payback period, US$9.25 million annual energy cost gain, US $0.014/kWh levelized cost of cooling, and US$0.015/kWh electricity capacities, outperform reference plants and the previous configurations. This is attributed to the higher thermal efficiency of solar hybrid PV-T systems, which reduces the solar field area requirement. Despite a higher cost per unit m^2 in the PVT system, the substantial electricity consumption effectively covers this cost, with excess electricity contributing to energy savings.

e) In comparison with the UCI Trigeneration Plant, the proposed system demonstrated remarkable enhancements, including a substantial increase in both annual electricity production and cooling capacity. The initial investment and operational expenses were significantly reduced, resulting in a considerably shorter payback period. Furthermore, the levelized costs of both electricity and cooling were markedly lowered, enhancing the system's overall financial viability. These combined improvements highlight the proposed system's superior capability to efficiently and cost-effectively meet high energy and cooling demands.

f) When compared with real-world data, the proposed system demonstrates higher performance metrics, particularly in COP and exergy efficiency. This suggests that the system could offer substantial advantages over conventional systems. CO_2 emissions were observed to be between 84.5 and 87.5 kg/MWh, aligning with the lower end of emissions reported for similar renewable energy systems. This demonstrates the system's potential for reducing greenhouse gas emissions in energy production. LCC and LCE were found to be competitive, with LCC ranging from $0.015 to $0.019/kWh and LCE between $0.0175 and $0.0195/kWh, both lower than the averages reported in comparable studies. These findings underscore the economic viability of the system.

g) Sensitivity analysis identified ambient temperature and solar radiation density as the most influential parameters on system performance. A 5 °C increase in ambient temperature decreased the COP by approximately 10 %, increasing the LCC by about 8 % and CO_2 emissions by around 6 %. This suggests that controlling ambient temperature is crucial for maintaining system efficiency and environmental benefits. Conversely, a 10 % increase in solar radiation density boosted energy production by 7 %, improved exergy efficiency by 5 %, and reduced LCE by 3 %, highlighting the importance of maximizing solar energy capture for optimal system performance.

h) To establish the optimum configuration of the proposed novel system, a single and multiobjective optimization process based on the exergoeconomic parameters was applied. The annual simulation results from TRNSYS indicate that the specified parameters—chosen for the third configuration of the proposed system at (130.18 °C, 35 °C, 42.98 °C, 24.68 °C, 15.02 °C, 150 °C)—result in a total annual electricity and cooling load production of 396.2 GWh and 59213.4 MWh, respectively.

i) The proposed system's environmental advantages were emphasized, particularly its role in cutting greenhouse gas emissions. By lowering CO_2 emissions to a range of 84.5 to 87.5 kg/MWh, the system supports broader efforts to address climate change, which is a central objective of the United Nations' Sustainable Development Goal (SDG) 13, advocating for immediate measures to combat climate change and its effects. The system's effective harnessing of solar energy was examined within the framework of SDG 7, which seeks to ensure universal access to affordable, reliable, and sustainable modern energy. By maximizing solar energy utilization and decreasing dependency on fossil fuels, the system aids in creating a cleaner energy portfolio, thereby fostering sustainability in energy production. The system's impact on water sustainability was explored, particularly regarding its lower water usage compared to conventional cooling systems. This contributes to SDG 6, which focuses on the sustainable management and availability of water and sanitation. The reduced water consumption of the proposed system helps ease the strain on water resources, a crucial consideration in regions with limited water availability. Furthermore, the system's economic feasibility was linked to SDG 9, which emphasizes the importance of industry, innovation, and infrastructure. With low levelized costs for cooling and electricity (ranging from $0.015 to $0.019/kWh for LCC and $0.0175 to $0.0195/kWh for LCE), the system demonstrates its capacity to support sustainable industrial practices and the development of infrastructure.

CRediT authorship contribution statement

Asli Tiktas: Writing – review & editing, Writing – original draft, Methodology, Investigation, Formal analysis, Conceptualization. **Huseyin Gunerhan:** Writing – review & editing, Writing – original draft, Supervision, Methodology, Investigation, Formal analysis, Conceptualization. **Arif Hepbasli:** Supervision, Methodology, Investigation, Formal analysis, Conceptualization.

Funding

This research did not receive any specific grant from funding agencies in the public, commercial, or not-for-profit sectors.

Declaration of competing interest

The authors declare that they have no known competing financial interests or personal relationships that could have appeared to influence the work reported in this paper.

Acknowledgements

The authors are very grateful to the reviewers and editor for their valuable and constructive comments, which led to increasing the quality

of the paper.

Data availability

Data will be made available on request.

References

[1] bp, 2023. bp Energy Outlook 2023.
[2] S. Quoilin, M.V.D. Broek, S. Declaye, P. Dewallef, V. Lemort, Techno-economic survey of organic rankine cycle (ORC) systems, Renew. Sustain. Energy Rev. 22 (2013) 168–186, https://doi.org/10.1016/j.rser.2013.01.028.
[3] O.G. Pop, A. Dobrovicescu, A. Serban, M. Ciocan, A. Zaaoumi, D.P. Hiris, M. C. Balan, Analytical modelling of food storage cooling with solar ammonia-water absorption system, powered by parabolic trough collectors, Method. *MethodsX* 10 (2023) 102013.
[4] S. Sigue, S. Abderafi, S. Vaudreuil, T. Bounahmidi, Design and steady-state simulation of a CSP-ORC power plant using an open-source co-simulation framework combining SAM and DWSIM, Therm. Sci. Eng. Prog. 37 (2023) 101580.
[5] D.O. Machado, W.D. Chicaiza, J.M. Escaño, A.J. Gallego, G.A. de Andrade, J. E. Normey-Rico, E.F. Camacho, Digital twin of a Fresnel solar collector for solar cooling, Appl. Energy 339 (2023) 120944.
[6] J.J. Díaz Carrillo, 2023. Solar thermal cooling systems driven by linear Fresnel collectors, realistic and practical simulation tool, cases studies applications and machine learning as a control approach. *Doctoral dissertation, Industriales*.
[7] A. Tiktaş, H. Gunerhan, A. Hepbasli, Exergy and sustainability-based optimisation of flat plate solar collectors by using a novel mathematical model, Int. J. Exergy 42 (2) (2023) 192–215.
[8] R. Nikbakhti, X. Wang, A.K. Hussein, A. Iranmanesh, Absorption cooling systems – Review of various techniques for energy performance enhancement, Alexandria Eng. J. 59 (2) (2020) 707–738, https://doi.org/10.1016/j.aej.2020.01.036.
[9] E. Elnagar, A. Zeoli, R. Rahif, S. Attia, V. Lemort, A qualitative assessment of integrated active cooling systems: a review with a focus on system flexibility and climate resilience, Renew. Sustain. Energy Rev. 175 (2023), https://doi.org/10.1016/j.rser.2023.113179.
[10] A. Tiktaş, H. Gunerhan, A. Hepbasli, E. Açıkkalp, Exergy-based techno-economic and environmental assessments of a proposed integrated solar powered electricity generation system along with novel prioritization method and performance indices, Process Saf. Environ. Prot. 178 (2023) 396–413, https://doi.org/10.1016/j.psep.2023.08.048.
[11] M. Wang, Y. Wang, X. Feng, C. Deng, X. Lan, Energy Performance comparison between power and absorption refrigeration cycles for low grade waste heat recovery, ACS Sustain. Chem. Eng. 6 (4) (2018) 4614–4624, https://doi.org/10.1021/acssuschemeng.7b03589.
[12] G. Mohan, S. Dahal, U. Kumar, A. Martin, H. Kayal, Development of natural gas fired combined cycle plant for tri-generation of power, cooling and clean water using waste heat recovery: techno-economic analysis, Energies 7 (10) (2014) 6358–6381.
[13] BOWLING GREEN STATE UNIVERSITY - CENTREX CENTRAL CHILLER PLANT - HAWA, 2016, Accessed: Oct. 12, 2023. [Online]. Available: file:///F:/Solar+ABSHeatCool%20Research%20Article/07.10.2023/BOWLING%20GREEN%20STATE%20UNIVERSITY%20-%20CENTREX%20CENTRAL%20CHILLER%20PLANT%20-%20HAWA.html.
[14] Chilled Water Plant Assessment & Criteria Design Cleveland Airport System, 2016, Accessed: Oct. 12, 2023. [Online]. Available: https://www.clevelandairport.com/sites/default/files/11_20_2018_osborn_report.pdf.
[15] P. Kumar, O. Singh, Thermoeconomic analysis of SOFC-GT-VARS-ORC combined power and cooling system, Int. J. Hydrogen Energy 44 (50) (2019) 27575–27586.
[16] A.S. Alsagri, A.A. Alrobaian, S.A. Almohaimeed, Concentrating solar collectors in absorption and adsorption cooling cycles: an overview, Energy Convers. Manage. 223 (2020), https://doi.org/10.1016/j.enconman.2020.113420.
[17] Integrated solar heating and cooling unit based on a novel zeolite chiller and heat pump, 2020, Accessed: Oct. 12, 2023. [Online]. Available: https://cordis.europa.eu/project/id/760210.
[18] S.A. Mousavi, M. Mehrpooya, A comprehensive exergy-based evaluation on cascade absorption-compression refrigeration system for low temperature applications - exergy, exergoeconomic, and exergoenvironmental assessments, J. Clean. Prod. 246 (2020), https://doi.org/10.1016/j.jclepro.2019.119005.
[19] X.D. Xue, T. Zhang, X.L. Zhang, L.R. Ma, Y.L. He, M.J. Li, S.W. Mei, Performance evaluation and exergy analysis of a novel combined cooling, heating and power (CCHP) system based on liquid air energy storage, Energy 222 (2021) 119975.
[20] J.C. César, J.C. Ortiz, G.V. Ochoa, R.R. Restrepo, J.R.N. Alvarez, A new computational tool for the development of advanced exergy analysis and LCA on single effect LiBr–H_2O solar absorption refrigeration system, Lubricants 9 (8) (2021) 76.
[21] F. Musharavati, S. Khanmohammadi, R. Tariq, Comparative exergy, multi-objective optimization, and extended environmental assessment of geothermal combined power and refrigeration systems, Process Saf. Environ. Prot. 156 (2021) 438–456.
[22] J. Wang, Z. Han, Y. Liu, X. Zhang, Z. Cui, Thermodynamic analysis of a combined cooling, heating, and power system integrated with full-spectrum hybrid solar energy device, Energy Convers. Manage. 228 (2021) 113596.
[23] A.M. Abed, H.S. Majdi, K. Sopian, F.H. Ali, M. Al-Bahrani, Q.R. Al-Amir, A. K. Yakoob, Techno-economic analysis of dual ejectors solar assisted combined absorption cooling cycle, Case Stud. Therm. Eng. 39 (2022) 102423.
[24] K.H. Chakravarty, M. Sadi, H. Chakravarty, A.S. Alsagri, T.J. Howard, A. Arabkoohsar, A review on integration of renewable energy processes in vapor absorption chiller for sustainable cooling, Sustain. Energy Technol. Assess. 50 (2022) 101822.
[25] U.R. Singh, A.S. Kaushik, S.S. Bhogilla, A novel renewable energy storage system based on reversible SOFC, hydrogen storage, Rankine cycle and absorption refrigeration system, Sustain. Energy Technol. Assess. 51 (2022), https://doi.org/10.1016/j.seta.2022.101978.
[26] S. Schüppler, P. Fleuchaus, A. Duchesne, P. Blum, Cooling supply costs of a university campus, Energy 249 (2022) 123554.
[27] Z. Tan, X. Feng, M. Yang, Y. Wang, Energy and economic performance comparison of heat pump and power cycle in low grade waste heat recovery, Energy 260 (2022), https://doi.org/10.1016/j.energy.2022.125149.
[28] B.J.R. Mungyeko Bisulandu, R. Mansouri, A. Ilinca, Diffusion absorption refrigeration systems: an overview of thermal mechanisms and models, Energies 16 (9) (2023) 3610.
[29] H. Caliskan, E. Açıkkalp, H.R. Takleh, V. Zare, Advanced, extended and combined extended-advanced exergy analyses of a novel geothermal powered combined cooling, heating and power (CCHP) system, Renew. Energy 206 (2023) 125–134.
[30] T. Zhou, J. Liu, J. Liu, J. Ren, S. Ding, S. Yang, Energy-exergy-economic-environmental (4E) analysis and multi-objective optimization of a cascade LiBr/H2O refrigeration and Organic Rankine cycle integrated system for power generation, Appl. Therm. Eng. 225 (2023) 120142.
[31] A. Razmi, M. Soltani, C. Aghanajafi, M. Torabi, Thermodynamic and economic investigation of a novel integration of the absorption-recompression refrigeration system with compressed air energy storage (CAES), Energy Convers. Manage. 187 (2019) 262–273.
[32] F.I. Abam, T.A. Briggs, O.E. Diemuodeke, E.B. Ekwe, K.N. Ujoatuonu, J. Isaac, M. C. Ndukwu, Thermodynamic and economic analysis of a Kalina system with integrated lithium-bromide-absorption cycle for power and cooling production, Energy Rep. 6 (2020) 1992–2005.
[33] M.R.M. Yazdi, F. Ommi, M.A. Ehyaei, M.A. Rosen, Comparison of gas turbine inlet air cooling systems for several climates in Iran using energy, exergy, economic, and environmental (4E) analyses, Energy Convers Manage. 216 (2020) 112944.
[34] M.G. Gado, S. Ookawara, S. Nada, I.I. El-Sharkawy, Hybrid sorption-vapor compression cooling systems: a comprehensive overview, Renew. Sustain. Energy Rev. 143 (2021) 110912.
[35] S.T. Kadam, A.S. Kyriakides, M.S. Khan, M. Shehabi, A.I. Papadopoulos, I. Hassan, P. Seferlis, Thermo-economic and environmental assessment of hybrid vapor compression-absorption refrigeration systems for district cooling, Energy 243 (2022) 122991.
[36] M. Mortadi, A. El Fadar, Performance, economic and environmental assessment of solar cooling systems under various climates, Energy Convers. Manage. 252 (2022) 114993.
[37] H. Zhang, X. Pan, J. Chen, J. Xie, Energy, exergy, economic and environmental analyses of a cascade absorption-compression refrigeration system using two-stage compression with complete intercooling, Appl. Therm. Eng. 225 (2023) 120185.
[38] M.T. Zun, M.S. Ahmad, H. Fayaz, J. Selvaraj, W. Ahmed, Y. Wang, B. Rashid, Towards techno-economics of green hydrogen as a primary combustion fuel for recreational vehicle vapor absorption refrigeration system, Sustainable Energy Technol. Assess. 56 (2023) 103007.
[39] A. Tiktas, H. Gunerhan, A. Hepbasli, E. Açıkkalp, Extended exergy analysis of a novel integrated absorptional cooling system design without utilization of generator for economical and robust provision of higher cooling demands, Energy. Convers. Manage. 307 (2024) 118350.
[40] A. Razmi, M. Soltani, M. Torabi, Investigation of an efficient and environmentally-friendly CCHP system based on CAES, ORC and compression-absorption refrigeration cycle: energy and exergy analysis, Energy Convers. Manage. 195 (2019) 1199–1211, https://doi.org/10.1016/j.enconman.2019.05.065.
[41] M.A. Emadi, N. Chitgar, O.A. Oyewunmi, C.N. Markides, Working-fluid selection and thermoeconomic optimisation of a combined cycle cogeneration dual-loop organic Rankine cycle (ORC) system for solid oxide fuel cell (SOFC) waste-heat recovery, Appl. Energy 261 (2020), https://doi.org/10.1016/j.apenergy.2019.114384.
[42] J. Li, M. Zoghi, L. Zhao, Thermo-economic assessment and optimization of a geothermal-driven tri-generation system for power, cooling, and hydrogen production, Energy 244 (2022), https://doi.org/10.1016/j.energy.2022.123151.
[43] X. Hong, F. Shi, Comparative analysis of small-scale integrated solar orc-absorption based cogeneration systems, Energies 13 (4) (2020) 946.
[44] DEWA Solar Innovation Centre., 2020. Accessed: Aug. 2, 2024, [Online]. Available: https://www.mbrsic.ae/en/about/sustainability-innovation-centre/.
[45] A. Piña-Martinez, S. Lasala, R. Privat, V. Falk, J.N. Jaubert, Design of promising working fluids for emergent combined cooling, heating, and power (CCHP) systems, ACS Sustain. Chem. Eng. 9 (35) (2021) 11807–11824.
[46] Y. Khan, R.S. Mishra, 2021. Parametric evaluation of solar driven combined supercritical organic Rankine cycle and vapor absorption refrigeration cycle for trigeneration. *Journal of Physics: Conference Series* (Vol. 1950, No. 1, p. 012034). IOP Publishing.
[47] J. García-Domínguez, A.M. Blanco-Marigorta, J.D. Marcos, Analysis of a solar driven ORC-absorption based CCHP system from a novel exergy approach, Energy Convers. Manage.: X 19 (2023) 100402.

[48] J.C. Jiménez-García, I. Moreno-Cruz, W. Rivera, Thermodynamic modeling of a solar-driven organic rankine cycle-absorption cooling system for simultaneous power and cooling production, Processes 12 (3) (2024) 427.
[49] O. Marc, F. Lucas, F. Sinama, E. Monceyron, Experimental investigation of a solar cooling absorption system operating without any backup system under tropical climate, Energy Build. 42 (6) (2010) 774–782.
[50] F. Cudok, J.C. Ciganda, N. Kononenko, E. Drescher, Experimental results of an absorption heat transformer, in: 12th IEA Heat Pump Conference, 2017, pp. 1–12.
[51] Y.C. Tsai, Y.Q. Feng, Y. Shuai, J.H. Lai, M.K. Leung, Y. Wei, T.C. Hung, Experimental validation of a 0.3 kW ORC for the future purposes in the study of low-grade thermal to power conversion, Energy 285 (2023) 129422.
[52] A. Tiktas, H. Gunerhan, A. Hepbasli, Single and multigeneration Rankine cycles with aspects of thermodynamical modeling, energy and exergy analyses and optimization: a key review along with novel system description figures, Energy Convers. Manage: X 14 (2022) 100199.
[53] UCI Energy Institute., 2022. UCI trigeneration plant: Overview and performance. *University of California, Irvine*, retrieved from https://www.energy.uci.edu/trigeneration-plant.
[54] C.T. Chong, Y. Van Fan, C.T. Lee, J.J. Klemeš, Post COVID-19 ENERGY sustainability and carbon emissions neutrality, Energy 241 (2022) 122801.
[55] T.G. Walmsley, M.R. Walmsley, P.S. Varbanov, J.J. Klemeš, Energy Ratio analysis and accounting for renewable and non-renewable electricity generation: a review, Renew. Sustain. Energy Rev. 98 (2018) 328–345.
[56] Y. Van Fan, J.J. Klemeš, S.R.W. Alwi, The environmental footprint of renewable energy transition with increasing energy demand: eco-cost, Chem. Eng. Trans. 86 (2021) 199–204.
[57] M. Baghsheikhi, M. Mohammadi, Experimental investigation of the vapor-compression cooling system in a data center: energy and exergy analysis, J. Therm. Anal. Calorim. 148 (17) (2023) 9079–9097.
[58] A. Saoud, Y. Boukhchana, A. Fellah, Thermal and parametric investigation of solar-powered single-effect absorption cooling system, J. Therm. Anal. Calorim. (2024) 1–16.
[59] D.K. Sharma, D. Sharma, A.H.H. Ali, A state of the art on solar-powered vapor absorption cooling systems integrated with thermal energy storage, Environ. Sci. Pollut. Res. 27 (1) (2020) 158–189.
[60] Fraunhofer Institute for Solar Energy Systems, 2020. Life cycle assessment of photovoltaic systems. *Fraunhofer ISE*, retrieved from https://www.ise.fraunhofer.de.
[61] National Renewable Energy Laboratory, 2020. Life cycle greenhouse gas emissions from solar photovoltaics. *NREL*, retrieved from https://www.nrel.gov.
[62] International Renewable Energy Agency, 2020. Renewable power generation costs in 2020. *IRENA*, retrieved from https://www.irena.org/Publications.
[63] United Nations., 2015. Transforming our world: The 2030 agenda for sustainable development. *United Nations General Assembly*. https://sdgs.un.org/2030agenda.